3-2022

Thermal Relaxation of Shot Peen Induced Residual Stresses in a Nickel-Base Superalloy

Bryce E. Van Velson

THERMAL RELAXATION OF SHOT PEEN INDUCED RESIDUAL STRESSES IN A NICKEL-BASE SUPERALLOY

THESIS

Bryce E. Van Velson, Captain, USAF

AFIT-ENY-MS-22-M-316

DEPARTMENT OF THE AIR FORCE
AIR UNIVERSITY

AIR FORCE INSTITUTE OF TECHNOLOGY

Wright-Patterson Air Force Base, Ohio

AFIT-ENY-MS-22-M-316

THERMAL RELAXATION OF SHOT PEEN INDUCED RESIDUAL STRESSES IN A NICKEL BASE SUPERALLOY

THESIS

Presented to the Faculty

Department of Aeronautics and Astronautics

Graduate School of Engineering and Management

Air Force Institute of Technology

Air University

Air Education and Training Command

In Partial Fulfillment of the Requirements for the

Degree of Master of Science in Aeronautical Engineering

Bryce E. Van Velson, BS, MSETM

Captain, USAF

March 2022

AFIT-ENY-MS-22-M-316

THERMAL RELAXATION OF SHOT PEEN INDUCED RESIDUAL STRESSES IN A NICKEL BASE SUPERALLOY

Bryce E. Van Velson, BS, MSETM

Captain, USAF

Committee Membership:

Dr. Anthony N. Palazotto
Chair

Dr. Marina B. Ruggles-Wrenn
Member

Maj John Brewer, PhD
Member

Abstract

Shot peening is a surface treatment used to improve the fatigue life of mechanical components that experience cyclic loading. The impact of shot causes plastic deformation on the surface of the part and just below, causing compressive residual stress. During the life cycle of a shot peened part, the residual stress will evolve due to thermal and mechanical relaxation. Understanding how residual stress behaves under thermal and mechanical loading will provide engineers and designers the ability to incorporate compressive residual stress into the design process.

This research investigates thermally activated relaxation of shot peen induced compressive residual stress in the powder metallurgy nickel-base superalloy ME3. Nickel-base superalloys are a category of material that have high tensile, creep, and fatigue properties which can be improved with surface treatments like shot peening, commonly used in applications such as turbine engine disks. Samples of ME3 were shot peened and exposed to high temperature environments, and the residual stress was measured using the hole drilling method and x-ray diffraction. The hole drilling method measures residual stress by measuring the strain caused when a hole is drilled into a surface that is under residual stress and calculating the stress from the strain. Surface and near surface relaxation behavior was quantified according to the Zener-Wert-Avrami function, and the evolution of the compressive residual stress was recorded. Applications for results generated in this research and recommendations for further research are discussed.

Acknowledgments

The personnel at AFRL/RX who have assisted me throughout this process have been indispensable. In particular, John Porter and Mark Ruddell with the University of Dayton Research Institute were very helpful with the thermal exposures, Joshua Ward with the Strategic Ohio Council for Higher Education provided much assistance with the hole drilling measurements, and Dr. Patrick Golden helped with much of the research process, guiding me in a direction that would make this research useful for AFRL and the Air Force at large.

Bryce E. Van Velson

Table of Contents

Page

List of Figures

Page

List of Tables

Page

THERMAL RELAXATION OF SHOT PEEN INDUCED RESIDUAL STRESSES IN A NICKEL BASE SUPERALLOY

I. Introduction

Research Objective

Compressive residual stresses are frequently induced through surface treatments such as shot peening to improve the fatigue life of components. [1] However, it is widely observed that these sorts of residual stresses will relax over time, and that high temperatures and mechanical loading will accelerate this relaxation. [2] Because of this, current best practice does not usually permit designers and engineers to consider the presence of these induced residual stresses in life calculations. The Air Force Research Laboratory Materials and Manufacturing Directorate (AFRL/RX) is currently investigating the ability to incorporate the effects of residual stress in turbine engine component design through the Advanced Lifing and Risk Management (ALARM) program. The ability to incorporate these effects into design tools requires a better understanding of shot peening process controls, residual stress measurement tools, and most especially, the relaxation behavior of residual stresses after thermal exposure and mechanical loading. The ALARM program focuses on tools for nickel-base superalloys, and in particular, the superalloy ME3. The objective of this research is to quantify the relaxation of shot-peen induced compressive residual stresses in the nickel base superalloy ME3.

Background

Nickel Base Superalloys and Powder Metallurgy

The term “superalloys” generally refers to a group of alloys designed to operate in high-temperature, corrosive environments at high stresses. These alloys typically have a base of nickel or cobalt. [3,4] Superalloys are often used in turbine engine disks, space vehicles, heat treating equipment, nuclear power systems, and other high-temperature environments. [5] Nickel base superalloys typically have a chromium content between 10% and 25%. The addition of iron can improve machinability and formability. [6] Superalloys exhibit high tensile, creep, and fatigue strength. [3]

These mechanical properties are improved through solid solution strengthening and precipitation hardening. Solid solution strengthening is the dissolving of other elements in solution. Molybdenum, tungsten, cobalt, vanadium, titanium, and aluminum are commonly used with nickel to achieve this strengthening. [5,6] This strengthening is due to differences in atomic diameter. The dissolved strengthening element will either become an interstitial atom, inserting itself between the crystal lattice, or a substitutional atom, replacing one of the base atoms in the crystal lattice. At high temperatures (above $0.6T_m$), large, slow diffusing elements such as molybdenum and tungsten are the most effective strengthening solutes. [5,6]

Precipitation hardening is a strengthening mechanism whereby a secondary phase precipitates out of the material and creates impurities in the microstructure that impede dislocation movement. Nickel-base superalloys are primarily γ phase, a face-centered cubic (fcc) austenitic phase, and the strengthening phase is primarily γ’ phase. The γ’ phase is an intermetallic phase that are precipitates of the form Ni_3(Al, Ti). [3,5,6] It is

also fcc, and typically has 1% or lower mismatch with the γ phase. This allows for low surface energy between the phases and long-term stability.[5]

Many superalloys can be, or even must be, produced using powder metallurgy. Powder metallurgy is used with alloy compositions that are difficult or impossible to cast with conventional melt and recast methods, and can produce finer grains than traditional casting procedures. [7] This is advantageous because material strength is related to grain size. Finer grains produce stronger materials. In general, powder metallurgy may be broken down into four steps: powder production, powder consolidation, thermomechanical processing, and heat treatment. [7]

The powders are produced in one of three ways: atomization, mechanically, or chemically. Atomization can be accomplished through several different means, but the goal for all of them is to melt the virgin material and disperse the melt into droplets so that it can solidify into a powder. One way in which this is accomplished is by using a secondary furnace to melt ingots and mix the alloying elements, then pass the melt through a small orifice and disintegrate the flow into droplets using a high-pressure stream of an inert gas (such as argon) so that it solidifies into a powder. Alternatively, an electric arc or plasma can melt a consumable anode under a vacuum or protective atmosphere and use centrifugal force to disintegrate the melted metal into droplets so that it can solidify into powder. [4,7] Yet another way to atomize the material is to saturate the molten metal with a gas such as hydrogen and spray it into a chamber under a dynamic vacuum. The rapid expansion of the gas in the vacuum will produce a fine spray of molten metal that then solidifies into a fine powder. [4] Mechanical powder production requires welding together constituent alloying elements, breaking it apart, and repeating

until the nominal alloy composition is achieved throughout. This workpiece is then dry milled to produce the powder. Chemical powder production precipitates the powder out from aqueous solution. [7] This is only used for alloys with simple matrices.

When the powder has been produced, it must be consolidated into a solid. In general, consolidation requires a way to enclose the powder, evacuate the gases in the enclosure, and then compact the powder into a solid. While extrusion and forging are possible [7], the most common method is hot isostatic pressing (HIP). In HIP, the powder is packed into a container (usually sheet metal) under a dynamic vacuum, sealed, evacuated of gas, heated, and then pressed with either a closed die or with high ambient pressure. This method can produce a fully dense final product without prior particle boundaries. Once the powder is consolidated into an ingot, conventional hot and cold working processes can be used on it [4,7] and it can be heat treated to develop desired microstructures. Solution annealing allows carbides and other precipitates to go into solid solution, while precipitation aging develops desired precipitate size and distribution. [7]

Residual Stress and Shot Peening

Residual stresses are self-equilibrating stress present in a member without any external load. There will be regions of compressive stress balanced by regions of tensile stress, so equilibrium is maintained in the member. There are several causes of residual stresses. The unequal rate of cooling between exterior and interior areas after casting, forging, extruding, and other heat treatments are one common cause. [8] Residual stress can also be induced through machining and cold work processes, including shot peening. [1,9] Compressive residual stresses in near surface areas have been shown to improve fatigue life. [1] Compressive residual stress near the surface means that more force is

required to place the part into tension required to form and open cracks. Crack formation and propagation is retarded by compressive residual stress by closing the crack tip. [10,11] Compressive residual stress can also mitigate other deleterious effects, such as damage from cavitation, fretting and fretting fatigue, galling, and stress corrosion cracking. [12]

Shot peening is one of the most common processes to induce compressive residual stresses in a part. It is a process by which small media, known as shot, are blasted against the surface of a part to induce residual stress. The impact from the shot produces small areas of tensile plastic deformation in the surface region. See Figure 1.

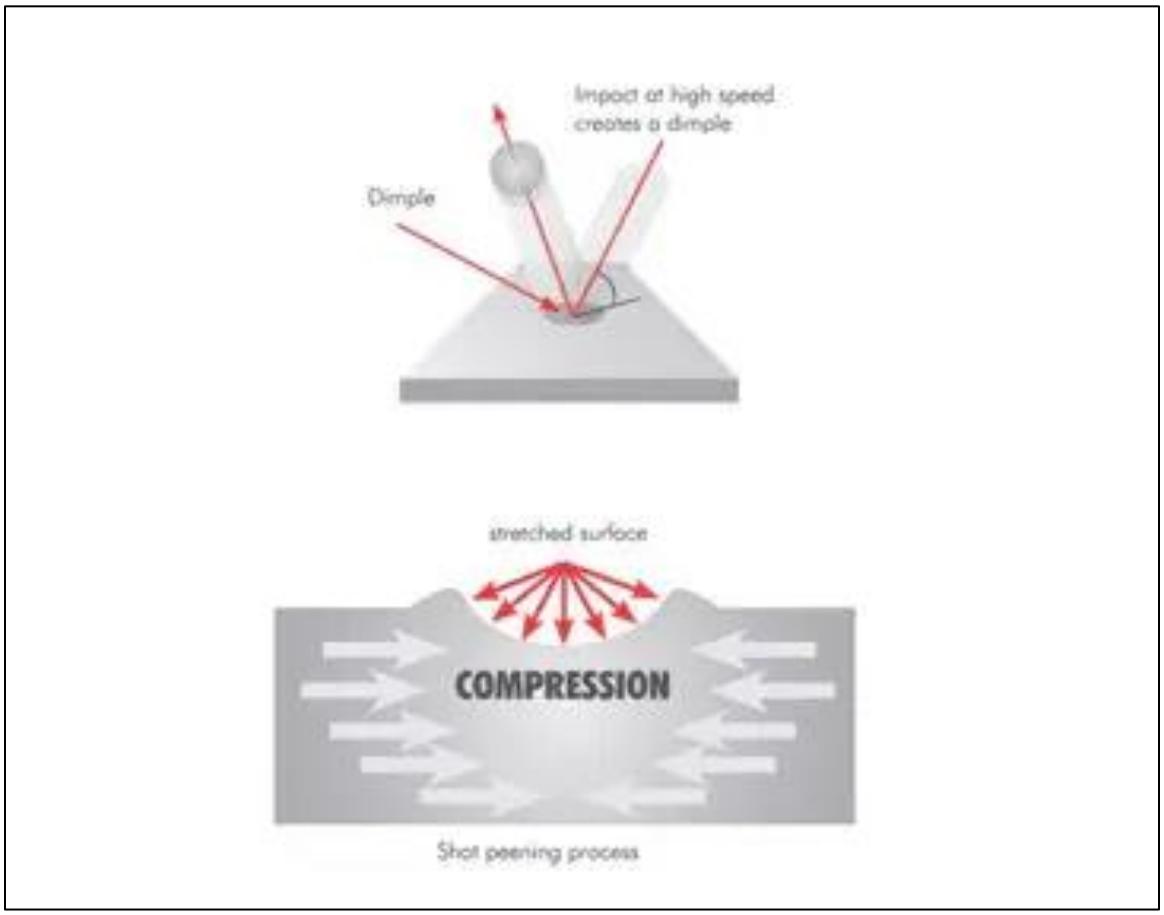

Figure 1 Diagram of shot peening process individual shot [13]

This tensile plastic deformation results in compressive residual stress in the surface and near-surface regions. The Heyn spring model demonstrates how this occurs. Consider three springs in parallel, with the center spring shorter than the external springs. Stretch the shorter spring to the length of the longer springs, thus putting it in tension. Attach the longer springs and release the system. The longer external springs will resist the tendency of the center spring to return to its original length. Thus, they are in compression. See Figure 2. The tensile plastic deformation experienced by the surface of a part during shot peening can be compared to the stretching of the shorter spring. The bulk of the material is trying to retain the original shape and opposes the plastic deformation. It is this resistance to plastic deformation that results in compressive stress near the surface. [1]

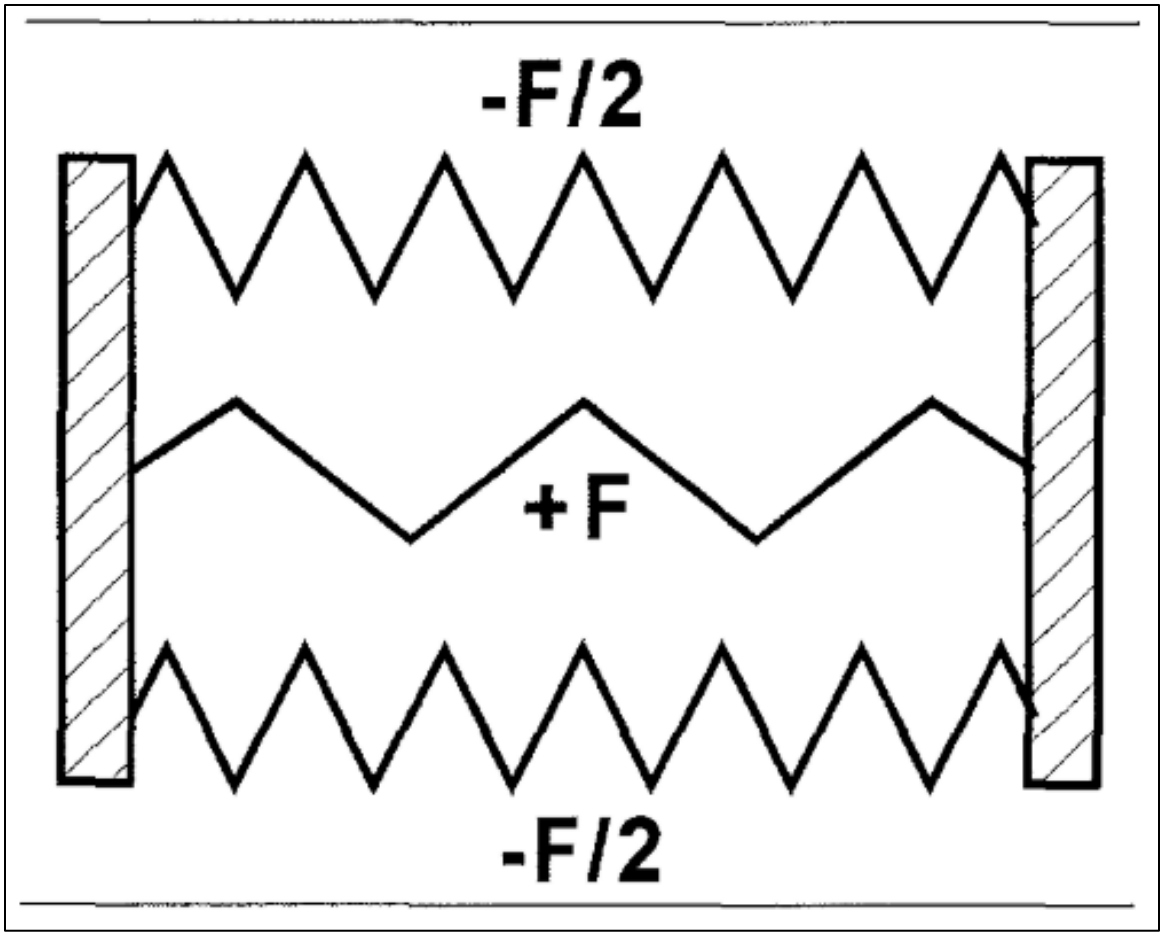

Figure 2 Heyn spring model [1]

Because there are regions of tension and compression that vary in size and distribution, there is necessarily a gradient, especially through the depth of a shot peened component. The Heyn model is a rheological explanation for how shot peening introduces residual stress, but there are also metallurgical reasons. The strength of materials is related to the ability of a material to prevent the movement of imperfections in the crystal lattice, especially dislocations. Virtually all strengthening mechanisms are based on the principle of improving a material's ability to restrict or hinder dislocation motion. Plastic deformation is due to dislocation movement, but plastic deformation also

causes dislocations to occur. The interaction between dislocations tends to impede the motion of dislocations, thereby strengthening the material. This interaction is the driving force behind strain hardening, especially at room temperatures. [10] Shot peening causes plastic deformation in the near surface areas, thus increasing dislocation density and strengthening the near surface area.

If we consider the uniaxial case on a stress-strain curve, the shot causes local plastic deformation, and there is a point in time where there is a peak loading. A portion of the strain induced by that peak load will be recovered through elasticity, but some elastic strain will be retained, as seen in Figure 3. This retained elastic strain is the difference between the total zero load strain and the plastic strain caused by the impact of the shot, and it is this retained elastic strain that causes residual stress. In the Heyn model, this retained elastic strain would be how much the central spring is still stretched after attaching the outer springs and allowing the system to come to equilibrium.

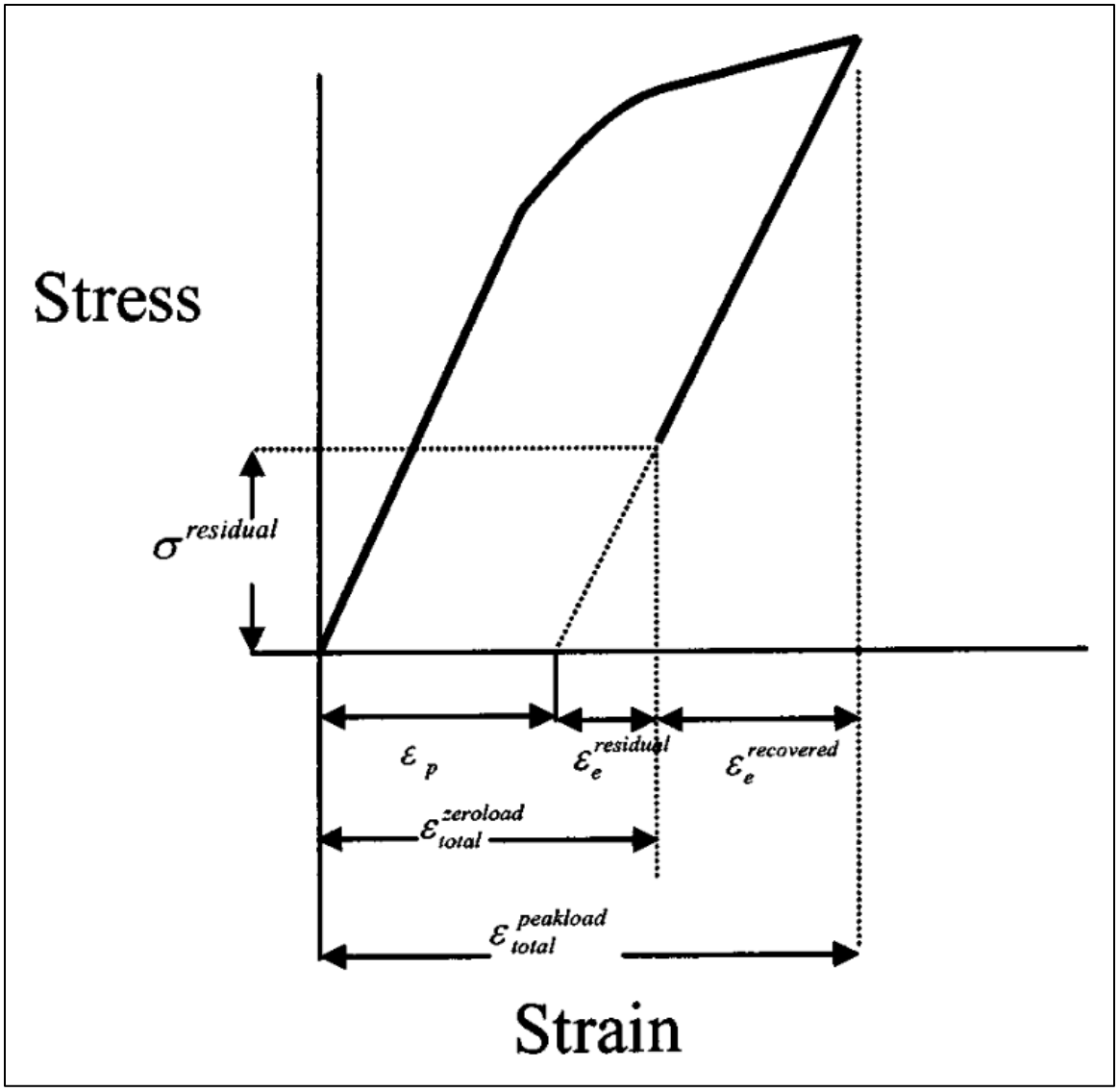

Figure 3 Total, elastic, and plastic strains, and residual stress [14]

The shot peening process is measured by saturation and controlled with Almen intensity. Saturation is the time (t) required to reach an Almen height that does not increase by more than 10% after twice that time (2t). The Almen height is the amount that a flat, rectangular piece of metal known as an Almen strip deflects from flat after peening. The Almen intensity is the intensity of shot peening (related to the size of the

shot, the speed that it hits the workpiece, the distance the workpiece is from the gun, etc) required to achieve a certain Almen height. [1]

Whether residual stresses have been deliberately imparted through a process like shot peening or are naturally occurring, it is often desirable to measure them. There are various methods that have been developed to measure these stresses, each of which have their own benefits and disadvantages. Rossini et al. [15] describe the most common methods in detail. These methods can be categorized as destructive, semi-destructive, or non-destructive. The destructive and semi-destructive methods rely on measuring the deformation due to the relaxation of the residual stresses when material is removed. These methods are also known as mechanical methods, and include the hole-drilling, ring-core, deep hole, sectioning, and contour methods. The most common destructive or semi-destructive method is the hole-drilling method. It is generally applicable to all materials, but it is especially useful for isotropic materials with known elastic parameters. A hole is drilled through the center of a specially designed strain rosette, the resultant strains measured, and the residual stresses calculated back from those strains. Non-destructive methods include X-ray and neutron diffraction, Barkhausen noise methods, and ultrasonic methods. These methods are often limited to laboratory settings or are limited in the type of material it can be used on. X-ray diffraction (XRD) is widely used and can be utilized in hand-held systems that make it possible to take measurements in the field. Externally applied or residual stresses are carried by the interatomic strains in the crystal lattice and deform. This elastic deformation causes changes to the interplanar spacing d of the crystal structure. By measuring the difference of d from d_0, the initial interplanar spacing, strain, and therefore stress, can be calculated. X-ray diffraction can

only measure residual stress at the surface, so measuring a residual stress profile through the depth of a part requires some material removal, usually through an acid etch.

Thermally Activated Relaxation

It is widely observed that residual stresses relax under thermal exposure, mechanical loading, and combinations thereof. [2] The application of thermal and/or mechanical energy converts elastic residual strains, ε_e, associated with residual stress according to Hooke's law into micro plastic strains, ε_p, through deformation processes such as dislocation slip, dislocation creep, and diffusion creep. [16] Dislocation slip and dislocation creep occur under mechanical loading, while diffusion creep, driven by the diffusion of atoms through the crystal lattice, occurs naturally without any external load, but usually does occur more readily with increasing temperature.

Several studies have shown that the thermal relaxation of residual stresses can be attributed to diffusion in the crystal lattice. In parts manufactured by cold gas dynamic spray (CGDS) also known as cold spray (CS), residual stresses form due to the plastic deformation of the powder particles that impact the surface of the substrate, and they can be relieved through a stress relieving heat treatment that also reduces or eliminates pores in the sprayed material through diffusion. [17,18] Similarly, it has been found in laser sintered parts that heat treatment can decrease grain boundary misorientation, which indicates decreased dislocation density and lower residual stresses. This can, in part, be attributed to the diffusion of atoms through the crystal lattice. [19] Chao et al. also found that stress relieving heat treatments relieved residual stresses through the rearrangement or annihilation of dislocations, due to the self-diffusion of various constituent elements. [20] In light of this, a brief discussion on diffusion is warranted.

While normally thought of as a process occurring between areas of two dissimilar metals, self-diffusion (that is, the motion of atoms in a pure metal) does occur. Steady state diffusion is described by Fick's first law:

$$J = -D\frac{dC}{dx} \tag{1}$$

where C is the atomic concentration, and the differential term represents the concentration gradient in the *x* direction. [10,21] However, this is only useful when the driving force is only a unidirectional concentration gradient. There may be other driving forces at work, such as elastic residual strains from plastic deformation, or there is more than one direction in which diffusion is occurring; in which case Fick's second law becomes more useful [10]

$$\frac{\partial C}{\partial t} = \frac{\partial}{\partial x_i}\left(D\frac{\partial C}{\partial x_i}\right) \tag{2}$$

In both of Fick's laws, the coefficient D is the diffusion coefficient, which is dependent on several variables, including the species diffusing and the temperature diffusion is occurring at. The temperature dependence of the diffusion coefficient [10,21] is

$$D = D_0 \exp\left(-\frac{Q_d}{RT}\right) \tag{3}$$

where D_0 is a temperature independent variable, Q_d is the activation energy for diffusion, R is the universal gas constant, and T is temperature. In any part, therefore, diffusion is a function of the activation energy for diffusion of the material and the temperature it is at. Two conditions must be satisfied for diffusion to occur: there must be space available for an atom to move into, and that atom must possess sufficient energy to move into the available space. Thus, there is an energy barrier that must be surmounted for any

individual atom to move from one location in the crystal lattice to another. Small activation free energies and high temperatures increase the rate of diffusion exponentially. [21] In the case of thermal relaxation of a shot peened metal alloy, the available space comes from the dislocations caused by the plastic deformation of the shot peening. The driving force becomes the elastic residual strains from the plastic deformation, and the thermal exposure increases the rate at which diffusion occurs. As diffusion occurs, atomic bonds under strain are relieved, either by being broken and reformed in an unstrained state, or by the removal of the dislocation that is causing the strain.

The macroscopic relaxation behavior of surface residual stresses is commonly observed to follow an exponential function known as the Zener-Wert-Avrami function. [2,16]

$$\frac{\sigma_{T,t}^{rs}}{\sigma_0^{rs}} = \exp[-(At)^m] \quad (4)$$

where A is also a function dependent on material properties and temperature according to

$$A = B\exp\left[-\frac{\Delta H}{kT}\right] \quad (5)$$

where B is a constant, ΔH is the activation enthalpy for relaxation, k is Boltzmann's constant, and T is the exposure temperature.

II. Literature Review

Chapter Overview

The purpose of this chapter is to review literature regarding the material under investigation, the nickel base superalloy ME3, and thermal relaxation of residual stresses in other nickel base superalloys. This material was developed by the National

Aeronautics and Space Administration (NASA), and much of the available literature on this material is from them. Because this kind of investigation has not been accomplished in this material before, the literature on thermal relaxation of residual stress in other nickel base superalloys will be reviewed.

Nickel-Base Superalloy ME3

The alloy used in the present work is known variously as ME3, ME16, and René 104. It was developed as a part of the NASA/General Electric/Pratt & Whitney High Speed Research/Enabling Propulsion Materials (HSR/EPM) program. It has moderately high γ' precipitate and refractory element content optimized with rapid cooling supersolvus heat treatment. [22,23] Typical chemical composition is shown in Table 1, and typical tensile data is shown in Table 2. This tensile data was used in the analysis in this work.

Table 1 Typical chemical composition of ME3[24]

ME3	Co	Cr	Ti	Mo	Al	Ta	W	Nb	Fe	C	Zr	Si	B	Ni
wt.%	20.6	13.0	3.7	3.8	3.4	2.4	2.1	0.9	0.03	0.05	0.045	0.03	0.02	Bal.
at. %	20.14	14.40	4.45	2.28	7.26	0.76	0.66	0.56	0.031	0.24	0.028	0.06	0.11	Bal.

Table 2 Typical tensile data for ME3[25]

	Yield (MPa/ksi)	UTS (MPa/ksi)	E (GPa/msi)	Elongation at break	Density (kg/m^3 / lb/in^3)
Fine Grain	1170/170	1680/244	220.6/32	24%	8304/0.3
Coarse Grain	1100/160	1585/230	220.6/32	20%	8304/0.3

Typical microstructural properties after a subsolvus heat treatment include mean grain sizes ASTM 11.9 to 12.1, with standard deviation ASTM 0.1 to 0.3 (4.9 to 5.2 μm). The as-large-as grain sizes were ASTM 7.3 to 8.5. The total γ' content has an area fraction 0.517 ± 0.008, with undissolved primary γ' having an area fraction of 0.152 ±

0.015 in the form of large particles 0.8 to 5 μm in diameter. Of the minor phases present, MC carbides are the predominant phase, comprising 88% of the total minor phase content. These carbides are 150 to 700 nm in diameter, and their qualitative phase chemistry is (Ti,Ta,Nb,Mo)C. The remaining 12% of the minor phases are M_3B_2 borides, ZrO_2 oxides, and Al_2O_3 oxides, with $(Mo,Cr,W)_3B_2$ making up 5%, ZrO_2 making up 5%, and Al_2O_3 making up the last 2%. At grain boundaries, $M_{23}C_6$ carbides dominated, mostly of the form $(Cr,Mo,W)_{23}C_6$, though larger MC carbides, M_3B_2 borides, ZrO_2 oxides, and Al_2O_3 oxides are also present.[22]

In one of their many studies of this material, NASA conducted tensile tests at temperatures ranging from 24°C to 816°C on both supersolvus and subsolvus heat treated samples. The strength of this material is strain rate dependent at temperatures 760°C and higher, decreasing with decreasing strain rate. The strain rate sensitivity increased with temperature and was slightly higher for the subsolvus heat treated material compared to the supersolvus teat treated material. Yield strength was sustained to about 704°C, then began to decrease with increasing temperature. Similarly, ultimate tensile strength was sustained to about 648°C and began to drop off after that point. In their conclusion, they recommended a maximum service temperature between 677°C and 704°C. [23]

Thermal Stability of Shot Peen Induced Residual Stress

In this context, thermal stability refers to the degree to which residual stresses are retained after exposure to high temperatures. An extensive review of the literature on the stability of mechanically induced residual stresses (such as through shot peening, low-plasticity burnishing, and other surface treatments, and through machining) during fatigue

and thermal exposure in common engineering alloys was conducted by McClung [2] in 2007, which reviewed most of the literature available at that time. In summary, it was found that residual stresses from shot peening in nickel-base superalloys generally relaxed between 50% and 75% after thermal exposures as short as one hour up to as long as 300 hours at temperatures ranging from 500°C and 704°C. Generally, residual stress relaxation increases with increased temperature, time, initial compressive stress, and initial cold work. The author noted that the temperatures used in these experiments are often unrealistically severe; however, gas turbine compressors and turbines can reach these temperatures and even hotter.

Since McClung wrote his review article, similar work has continued and shown qualitatively similar results. Buchanan et al.[26] investigated thermal relaxation of residual stress in Inconel 100 (IN100) in 2008. They subjected 40 mm x 49 mm x 4 mm plates of IN100 to shot peening at an Almen intensity of 6A with 125% coverage, and then used electrodischarge machining (EDM) to cut these plates into nine 13 mm x 16 mm samples. After peening, they exposed these sample to high temperature environments for up to 300 hours and measured the residual stress profiles in the samples with XRD. They found that for IN100, the residual stress imparted by shot peening relaxes by approximately 35% after a 300 hour exposure at 650°C and approximately 38% after a 300 hour exposure at 704°C. They also found that the stress relaxation behavior at the surface is not indicative of stress relaxation behavior in the interior of the sample, and that surface measurements alone should not be incorporated into fatigue life predictions.

Similarly, Foss et al. [27] investigated residual stress relaxation in the nickel base superalloy RR1000. Specimens measuring 15 mm x 15 mm x 2 mm were cut from larger

shot peened starting specimens and subject to thermal exposure at 700°C in oxidizing and high-vacuum environments for 48 hours. Residual stress was measured by XRD with electrolytic layer removal. They found that the oxidizing environment had no effect on the residual stress relaxation compared to the high-vacuum environment. The surface residual stresses relaxed by 63% and the maximum residual stresses relaxed by 38%. They also observed that depth at which the maximum residual stress occurs shifts from 50 μm to 75 μm, but the depth that the compressive residual stresses occur does not change and remains at approximately 200 μm.

Wu and Jiang [28] researched residual stress relaxation in Inconel 625 after thermal exposure at 500°C, 600°C, and 700°C. Samples of Inconel 625 were cut into 20 mm x 15 mm x 5 mm plates and heat treated before a dual shot peening process was carried out. The shot peened samples were then exposed to the referenced temperatures for time periods as short as one minute and as long as 120 minutes. Before 10 minutes of exposure, there were very few observable differences in the relaxation behavior at the different temperatures, but after 15 minutes, the surface compressive residual stress relaxed by 42%, 60%, and 79% at 500°C, 600°C, and 700°C, respectively. After the full two hours, the relaxation was 70%, 81%, and 86%. The maximum compressive residual stress relaxed by 32%, 37%, and 53% at 500°C, 600°C, and 700°C, respectively. Similar to the results reported by Foss et al., the maximum compressive residual stress occurred further from the surface after thermal exposure, and the compressive residual stresses only occurred within 200 μm of the surface.

Chin et al [29] investigated thermal relaxation of shot peen and laser shock peen induced residual stress in Inconel 718. Laser shock peening is a surface treatment similar

to shot peening that uses a laser and an overlay to create a plasma that generates shock waves in the material. See Figure 4

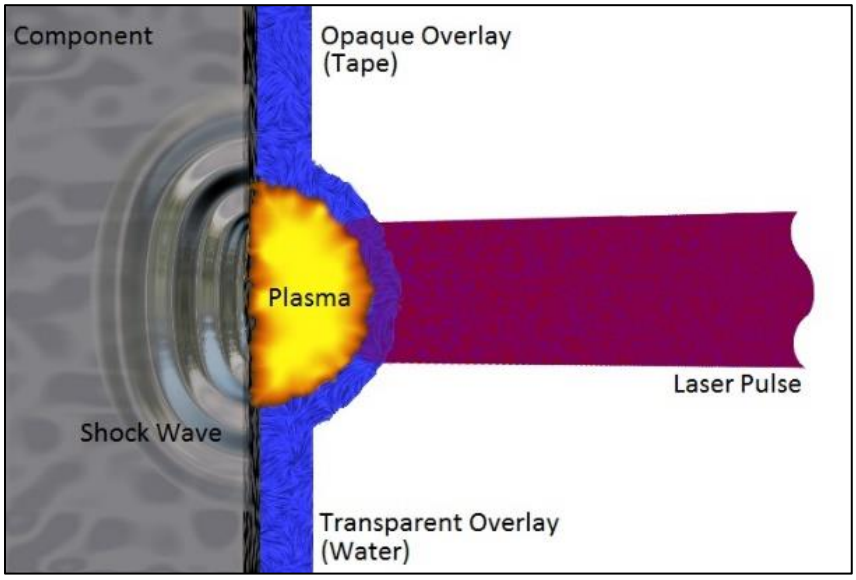

Figure 4 Diagram of laser shock peening single burst [30]

They shot peened and laser shock peened flat bars, then cut them into 20 mm x 20 mm squares and exposed them at temperatures of 250°C, 400°C, and 600°C for up to 20 hours. Residual stress was measured with XRD. Under thermal exposure, the shot peened samples consistently displayed more relaxation than the laser shock peened samples. At 600°C, surface residual stress in the shot peened samples relaxed by almost 45% after one hour of exposure, while the laser peened samples only experienced 10% surface relaxation. Significant relaxation continued at the surface for the shot peened samples for continued exposure to 10 hours, but there was limited further relaxation for the laser shock peened samples. After 10 hours at 600°C, the maximum residual stress had relaxed by 30% in the shot peened samples, as well as shifted from 80 μm to 100 μm. Subsurface residual stress in the laser shock peened samples only experienced minimal relaxation. At

the lower temperatures, relaxation was less than that at 600°C, even for longer exposure times. At the lower temperatures, the maximum relaxation for both the shot peened and the laser shock peened samples was only about 20%.

Chin et al also quantified the percent cold work accomplished by the shot peening and observed that there was a correlation between the initial cold work and the relaxation of the corresponding residual stress. The initial percent cold work was determined at each depth from the surface that residual stress was measured, and the retained residual stress after exposure was plotted against percent cold work. A linear relationship with R^2 greater than 0.85 was found for each exposure, and a modification to the Zener-Wert Avrami function was proposed to account for this. An additional coefficient C is introduced to the equation: $C = 1 - \alpha W$. The α term is a fitting parameter, and the W term is the initial cold work. This modification to the ZWA function produced a model with good correlation to experimental results at the lower temperatures of 250°C and 400C, but overestimates relaxation after exposure at 600°C. The authors attributed this to a different relaxation mechanism at 600°C that has different microstructural kinetics, and this model with the cold work term does not account for that.

III. Methodology

Experimental Procedures

The relaxation of residual stress was quantified by shot peening samples of ME3, exposing them to different temperatures for different lengths of time, and measuring the residual stress after thermal exposure using the hole drilling method and x-ray diffraction (XRD). The ME3 used in this project was purchased from Wyman-Gordon as 12.25”

diameter blanks weighing 300 lb each. They were forged into pancakes 3” thick and 20” in diameter by Pratt & Whitney Georgia Forgings Business. These blanks were forged at 1975°F at a nominal strain rate of 0.2 in/in/min. Bricks approximately 2” x 4” x 1” were then wire EDM cut from these forgings and subsequently heat treated to achieve a subsolvus microstructure and to remove residual stresses related to the original forging and removal from the block. Each of these heat-treated bricks was then wire EDM cut down further into four sample plates approximately 50 mm x 50 mm x 12 mm. Other bricks were also heat treated and subsequently cut into round samples for the purpose of tensile testing. Scrap from the tensile testing samples were mounted for scanning electron microscopy.

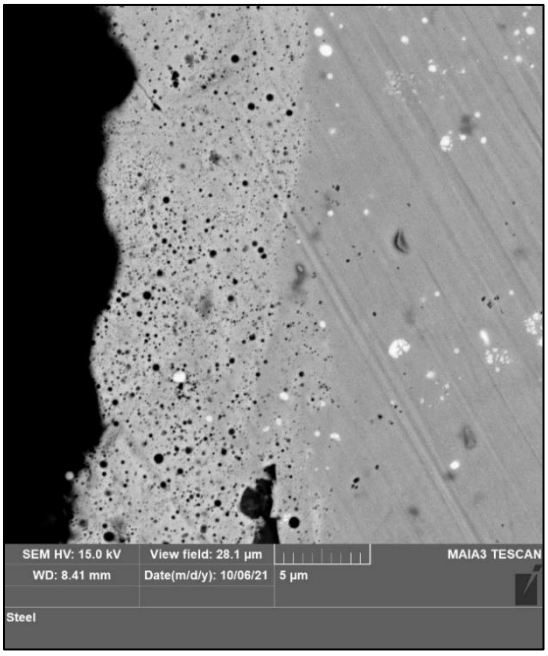

Figure 5 Scanning electron microscope image of typical EDM recast layer

Scanning electron microscopy was used to determine the thickness of the EDM recast layer so that the recast layer could be removed from the sample plates to provide a clean surface for shot peening. As seen in Figure 5, the EDM recast layer exhibited

porosity that would not have reacted to shot peening in the same way that the base metal would have, so it was necessary to remove it. The EDM recast layer was removed with grinding procedures based in the low-stress Metallic Test Specimen Preparation procedures from AFRL. [31] Empty metallographic mounts were adhered to the sample blanks to use as handles (see Figure 6).

Figure 6 Sample blank with metallographic mount handle for grinding

Grinding wheels and roll grinders with 120 to 600 grit papers were used for this process. After grinding with 120 grit paper for some time, an area with a rippled appearance typically appeared on the surface being ground. See Figure 7. This was an artifact of the EDM used to cut the bricks into plates. The plates were ground on the grinding wheel with 120 grit paper until these ripples disappeared. After that, the samples were ground on roll grinders with 240, 360, 400, and 600 grit papers. Grit was increased when the marks from the previous size grit were no longer visible. However, the intent

was not to polish the surface, but to remove the recast layer. When a clean, but not necessarily smooth, surface was achieved with 600 grit, the plate was considered to be finished.

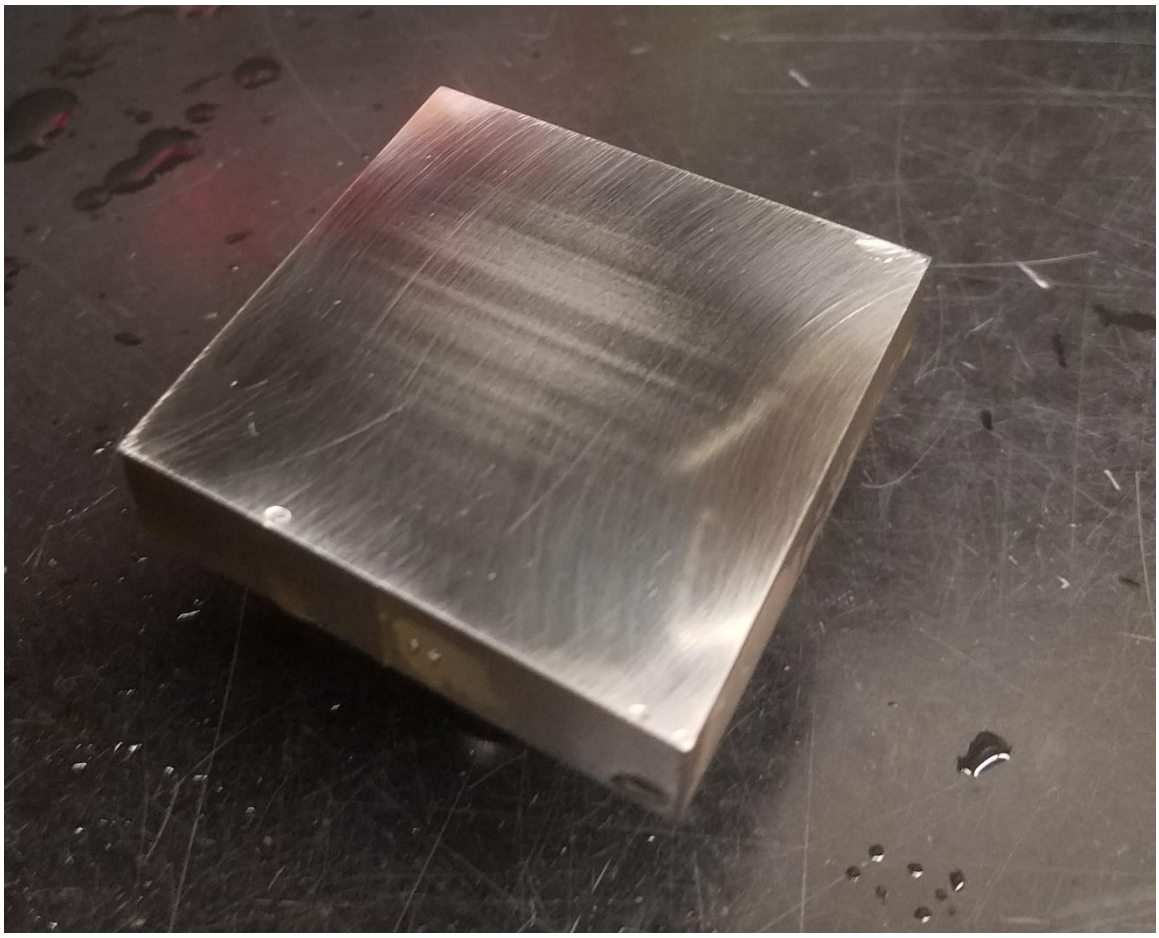

Figure 7 Partially ground sample plate showing rippled appearance

After the EDM recast layer was removed from the blanks, they were sent to be shot peened to 6-8 A in accordance with AMS-2430-U using ASR-170 shot media and peened to 125% coverage minimum. Peening was performed by Peening Technologies using a CNC process control to achieve specified peening conditions.

After peening, the sample blanks were cut into quarters so that the samples were approximately 25 mm x 25 mm x 12 mm. Some of these samples were then subjected to thermal exposures ranging from one hour to 300 hours, while others were left in the as peened state as either the control group or reserve samples. The matrix of times and temperatures for the thermal exposures is shown in Table 3.

Table 3 Matrix of time and temperature for thermal exposures

Exposure Time (hr)	N/A			538°C			650°C			704°C		
	HD	HD-Hill	XRD	HD	HD-Hill	XRD	HD	HD-Hill	XRD	HD	HD-Hill	XRD
0	3	2	1									
1				3	2	1	2	1	0	3	2	1
3										2	1	0
10										2	1	0
100				3	0	0	3	2	1	1	1	1
300							2					

The furnaces used were allowed to come to temperature before the samples were inserted. After the samples were inserted, the furnace was allowed to return to the nominal temperature before the exposure time began. This return to temperature typically took between 30 and 40 minutes. These temperatures were chosen because they are representative of conditions in the compressors and turbines of gas turbine engines. Residual stress was measured using the hole drilling method at AFRL/RX. Additional samples also received thermal exposure and were sent to Hill Engineering for additional hole drilling measurements and to Lambda Research, Inc for x-ray diffraction measurements. The hole drilling method requires some training and experience to produce consistent results. The measurements taken by Hill Engineering and Lambda Research Inc. will be used as a baseline to compare measurements taken at AFRL/RX.

Each sample was identified by the heat treatment number, the brick the sample blank was cut from (a, b, or c), the sample plate itself (A, B, C, or D), and a sequential identifier (1, 2, 3, or 4); e.g., 4061b.D.4.

Hole Drilling Method

In this present work, the hole drilling method was used to measure residual stress. The history, development, mathematical formulations, and use of the hole drilling method for measuring residual stress is described in detail in Ref [32], and it is standardized in the ASTM Standard Test Method E837. [33]

The strain gage rosettes used in the hole drilling method are specially designed to be able to drill through the center of the rosette. Standardized hole drilling strain gauge rosettes are shown in Figure 8. Type A rosettes, shown at the left of Figure 8, have gauges arranged at 0°-90°-225° (clockwise) or 0°-135°-270° (counterclockwise), and Type B rosettes, shown in the center of Figure 8, have gauges arranged at 0°-45°-90°. These types of rosettes have radial gauge elements that are used to calculate the strain components ε_x, ε_y, and γ_{xy}, and then apply Hooke's law to find the in-plane stress components σ_x, σ_y, and τ_{xy}. Type C rosettes, shown at the right of Figure 8, have three radial gauges and three tangential gages connected in three half-bridge circuits to increase effective strain sensitivity and compensates for thermal strains. They are used mostly with materials with low thermal conductivity such as plastics. Type A rosettes were used in the present work. Standard Type A rosettes come with nominal diameters of 1/32", 1/16", and 1/8", though the final drilled holes are usually slightly larger than the nominal, typically about 1 mm, 2 mm, and 4 mm, respectively. The rosettes, manufactured by

Micro-Measurements, were installed on the samples in accordance with the instructions in Micro-Measurements Bulletin B-127. [34]

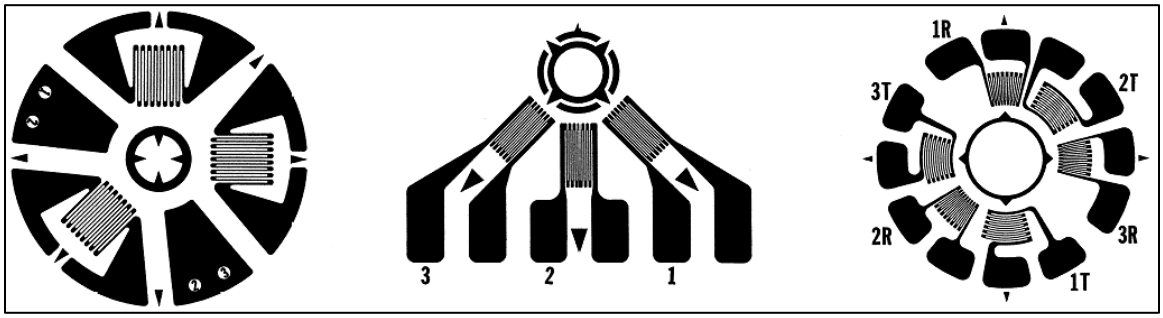

Figure 8 Standardized strain gauge rosettes used in the hole drilling method[32]

When the hole is drilled, the residual stresses will be relieved, and strains will be measured by the gauges in a radial direction. These strains are related to the in-plane stress tensor according to

$$\epsilon(\theta) = \left(\sigma_x + \sigma_y\right)A + \left(\sigma_x - \sigma_y\right)B\cos 2\theta + \tau_{xy}\sin 2\theta \tag{6}$$

where Θ is the angle counter-clockwise from the *x* direction. Equation (6) is derived from coordinate transformations and an application of Hooke's law. The values *A* and *B* are constants whose values are dependent on the depth and diameter of the hole drilled and the elastic properties of the material. Nominally, they should have the values

$$A = -\frac{1-\nu}{4E} \tag{7a}$$

$$B = -\frac{1+\nu}{4E} \tag{7b}$$

but because the gauges are measuring strains remotely, they tend to differ greatly from these values. Further, there is a 1+ν influence on the constant A that is an artifact of classical Kirsch analytical solutions for stress and strain around a hole in stressed

material. With these facts in mind, it is more convenient to nondimensionalize the calibration constants into $\bar{a}$ and $\bar{b}$

$$\bar{a} = \frac{2AE}{1+\nu} \tag{8a}$$

$$\bar{b} = 2BE \tag{8b}$$

so that the stress-strain relationship given in equation (6) becomes

$$\epsilon(\theta) = \frac{P\bar{a}(1+\nu)}{E} + \frac{Q\bar{b}\cos 2\theta}{E} + \frac{T\bar{b}\sin 2\theta}{E} \tag{9}$$

where, for simplifying future computations,

$$P = \frac{\sigma_x+\sigma_y}{2} \tag{10a}$$

$$Q = \frac{\sigma_x-\sigma_y}{2} \tag{10b}$$

$$T = \tau_{xy} \tag{10c}$$

The stress *P* is the isotropic component of stress, and the stresses *Q* and *T* are deviatoric components. The strains measured by the gauges of a Type A rosette are at 0°, 135°, and 270°, so these strains are given from equation (9) by

$$\epsilon_1 = \frac{P\bar{a}(1+\nu)}{E} + \frac{Q\bar{b}}{E} \tag{11a}$$

$$\epsilon_2 = \frac{P\bar{a}(1+\nu)}{E} - \frac{T\bar{b}}{E} \tag{11b}$$

$$\epsilon_3 = \frac{P\bar{a}(1+\nu)}{E} - \frac{Q\bar{b}}{E} \tag{11c}$$

which can be solved for P, Q, and T,

$$P = \frac{E}{\bar{a}(1+\nu)}p \tag{12a}$$

$$Q = \frac{E}{\bar{b}}q \tag{12b}$$

$$T = \frac{E}{\bar{b}}t \tag{12c}$$

with corresponding combined strains p, q, and t.

$$p = \frac{(\epsilon_1+\epsilon_2)}{2} \tag{13a}$$

$$q = \frac{(\epsilon_1-\epsilon_3)}{2} \tag{13b}$$

$$t = \frac{(\epsilon_1+\epsilon_3-2\epsilon_2)}{2} \tag{13c}$$

So, to measure the residual stress using the hole drilling method, a hole is drilled through the center of the strain gage rosette. The strain in each gage is measured, and the combined strains p, q, and t are calculated. From these combined strains, the combined stresses P, Q, and T are calculated by multiplying the combined strains by Young's modulus, scaled with calibration constants and Poisson's ratio as required. Once these combined stresses are acquired, the in-plane stress components are simply calculated by

$$\sigma_x = P + Q \tag{14a}$$

$$\sigma_y = P - Q \tag{14b}$$

$$\tau_{xy} = T \tag{14c}$$

This procedure will work as described to calculate the average uniform stress through the depth of the hole, but a non-uniform residual stress profile must be calculated incrementally, and the residual stress calculations must be done for each depth increment. This requires modifying equations (12a), (12b), and (12c) to take on the form of a summation:

$$p_i = \frac{1+\nu}{E}\sum_{j=1}^{j=i} \bar{a}_{ij}P_j \tag{15a}$$

$$q_i = \frac{1}{E}\sum_{j=1}^{j=i} \bar{b}_{ij}Q_j \tag{15b}$$

$$t_i = \frac{1}{E}\sum_{j=1}^{j=i} \bar{b}_{ij}T_j \tag{15c}$$

where p_i, q_i, and t_i are the strains measured after drilling to a hole depth increment *i*, P_j, Q_j, and T_j are the uniform stress within the hole depth increment *j*, and $\bar{a}_{ij}$ and $\bar{b}_{ij}$ are the calibration constants for each depth increment *j* of a hole *i* increments deep. The ASTM Standard Test Method E837 specifies 20 increments. After measuring the strain, the standard errors in the combined strains for each increment are also calculated. These are given by

$$p_{std}^2 = \sum_{j=1}^{n-3} \frac{\left(p_j - 3p_{j+1} + 3p_{j+2} - p_{j+3}\right)^2}{20(n-3)} \tag{16a}$$

$$q_{std}^2 = \sum_{j=1}^{n-3} \frac{\left(q_j - 3q_{j+1} + 3q_{j+2} - q_{j+3}\right)^2}{20(n-3)} \tag{16b}$$

$$t_{std}^2 = \sum_{j=1}^{n-3} \frac{\left(t_j - 3t_{j+1} + 3t_{j+2} - t_{j+3}\right)^2}{20(n-3)} \tag{16c}$$

where *n* is the number of sets of strain data at each depth increment. The stress calculations are simplified by considering them in matrix form:

$$\bar{\boldsymbol{a}}\boldsymbol{P} = \frac{E}{1+\nu}\boldsymbol{p} \tag{17a}$$

$$\bar{\boldsymbol{b}}\boldsymbol{Q} = E\boldsymbol{q} \tag{17b}$$

$$\bar{\boldsymbol{b}}\boldsymbol{T} = E\boldsymbol{t} \tag{17c}$$

Where the stresses and strains are vectors and the calibration constant matrices are lower-diagonal matrices.

Prior to 2020, the calibration constants had been calculated and standardized in ASTM Standard Test Method E837. In the 2020 revision, a method for calculating the calibration constants based on the dimensions of the sample was standardized. To calculate the calibration constants for a "thick" workpiece as defined in the standard, a 15 term, 5th order binomial equation in terms of the ratio of the hole depths h_j to the hole

diameter D and the stress depths H_k to D is used. For example, for a_{jk}, where *k* is the current hole depth increment and *j* is every hole depth increment up to *k*,

$$a_{jk} = c_1\left(\frac{H_k}{D}\right) + c_2\left(\frac{H_k}{D}\right)^2 + c_3\left(\frac{H_k}{D}\right)\left(\frac{h_j}{D}\right) + c_4\left(\frac{H_k}{D}\right)^3 + c_5\left(\frac{H_k}{D}\right)^2\left(\frac{h_j}{D}\right) + c_6\left(\frac{H_k}{D}\right)\left(\frac{h_j}{D}\right)^2 + c_7\left(\frac{H_k}{D}\right)^4 + c_8\left(\frac{H_k}{D}\right)^3\left(\frac{h_j}{D}\right) + c_9\left(\frac{H_k}{D}\right)^2\left(\frac{h_j}{D}\right)^2 + c_{10}\left(\frac{H_k}{D}\right)\left(\frac{h_j}{D}\right)^3 + c_{11}\left(\frac{H_k}{D}\right)^5 + c_{12}\left(\frac{H_k}{D}\right)^4\left(\frac{h_j}{D}\right) + c_{13}\left(\frac{H_k}{D}\right)^3\left(\frac{h_j}{D}\right)^2 + c_{14}\left(\frac{H_k}{D}\right)^2\left(\frac{h_j}{D}\right)^3 + c_{15}\left(\frac{H_k}{D}\right)\left(\frac{h_j}{D}\right)^4 \quad (18)$$

and similar for b_{jk}.[33] The coefficients c_i were determined numerically for each rosette type and are tabulated in ASTM E837. For "thin" and "intermediate" workpieces as defined by the standard test method, interpolations must be used, and are also described in the standard.

Figure 9 Hill Engineering DART machine [35]

In this work, the hole drilling accomplished at AFRL/RX used the Hill Engineering Device for Automated Residual stress Testing (DART) machine, shown in Figure 9. [36] The approximately 25 mm x 25 mm samples were secured in a table-top

drill press vice, and the vice was secured in the machine using accompanying fixtures. A support piece was cut from available scrap material and made level. This allowed the sample to sit in the vice so that it could be gripped with just enough purchase on the sample to hold it in place. This was necessary because using excessive force to hold the sample would induce strain in the sample. The instructions for the DART machine state to ensure that the part to be tested is fixed in the machine with less than 7 microstrain read by the data acquisition system. After ensuring that the sample is in place, the endmill used to cut the hole is centered over the rosette, oriented perpendicular to the sample, and carefully lowered to the surface of the sample. The film of the rosette is carefully cut through to begin drilling at the surface of the part, and when the machine is started, drilling and strain measurements are done automatically. After gathering the strain data, the residual stress is calculated automatically, and a report is generated. This report includes the strain data, the calculated stress, and its uncertainty.

IV. Analysis and Results

Hole Drilling Results

In most of the literature on residual stress relaxation, the magnitude of the surface residual stresses due to shot peening is typically smaller than that of the maximum compressive residual stress below the surface. The residual stress then decreased in magnitude further into the depth before eventually turning tensile below the surface to bring the system into equilibrium, such as can be seen in Figure 10, adapted from Ref [26]. It was observed in this work that the maximum compressive residual stress was

typically the first reported residual stress value. This is because the first reported residual stress value was below the surface, so surface stresses could be lower.

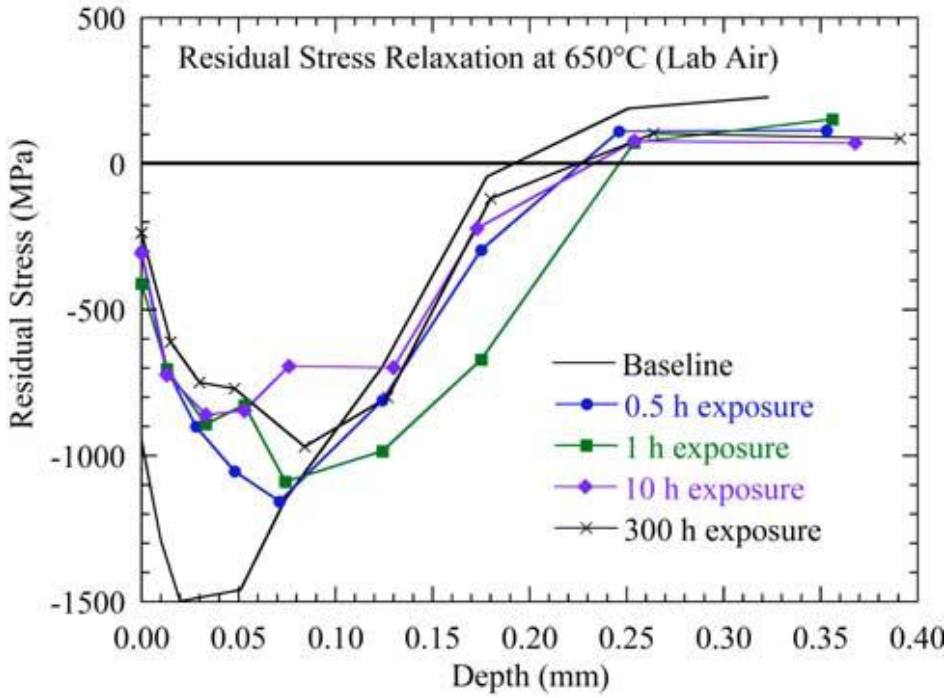

Figure 10 Residual stress distributions in IN100 versus exposure time at 650°C [26]

In shot peened parts like these samples, the residual stress is theoretically equal in all directions, so the average of the normal components σ_x and σ_y was used to determine the thermal relaxation. There was always some difference in the values of these two normal components, so some shear stress was measured. These differences could have various causes, such as the adherence of the rosette or relaxation induced by cutting the sample blanks into quarters. However, this shear is negligible compared to the normal components. The hole drilling results for each sample are shown in Figure 11 through Figure 20. Triangle data points come from Hill Engineering, and circle data points come from AFRL/RX. Generally, the measurements by Hill Engineering showed a higher magnitude of compressive residual stress, indicating less relaxation.

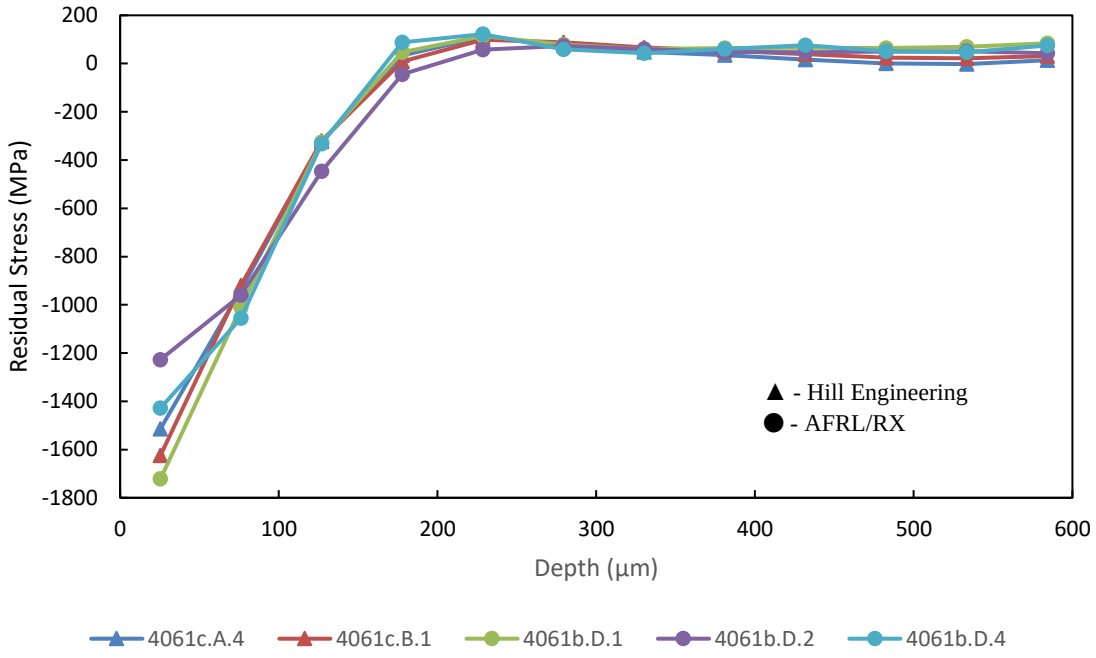

Figure 11 Residual stress profiles of the as-peened condition

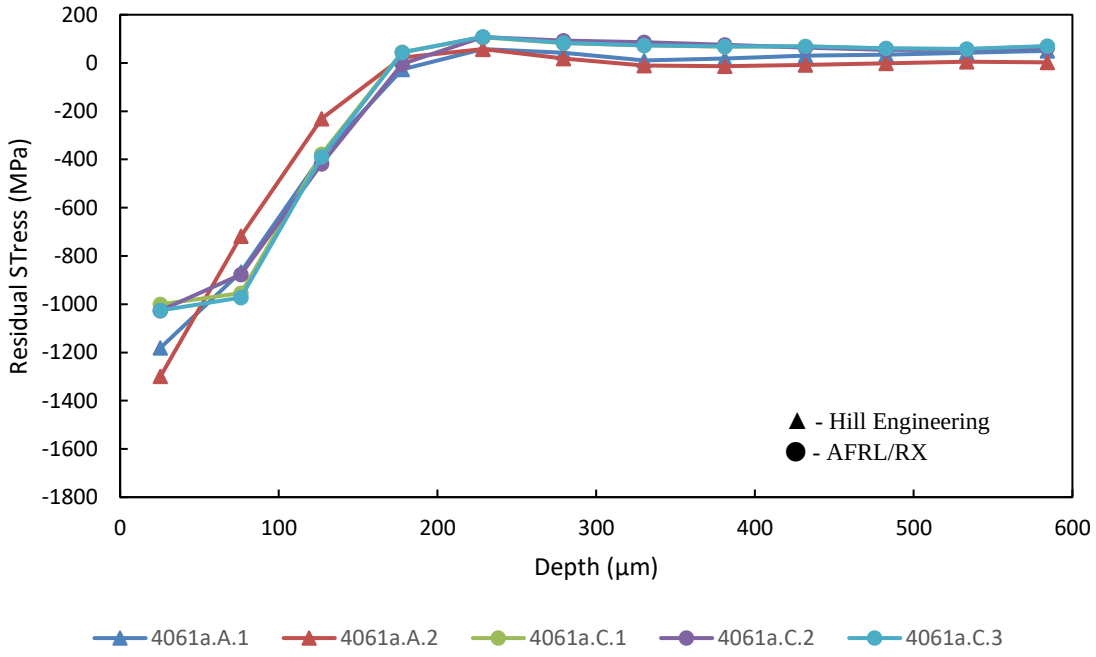

Figure 12 Residual stress profiles after thermal exposure at 538°C for 1 hour

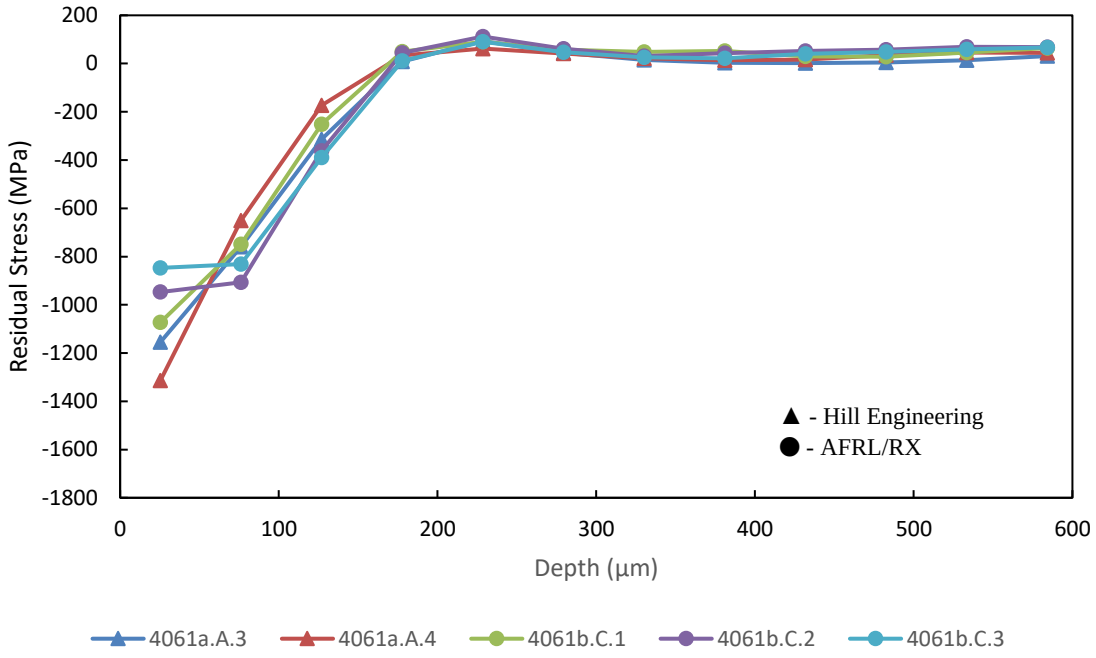

Figure 13 Residual stress profile after thermal exposure at 538°C for 100 hours

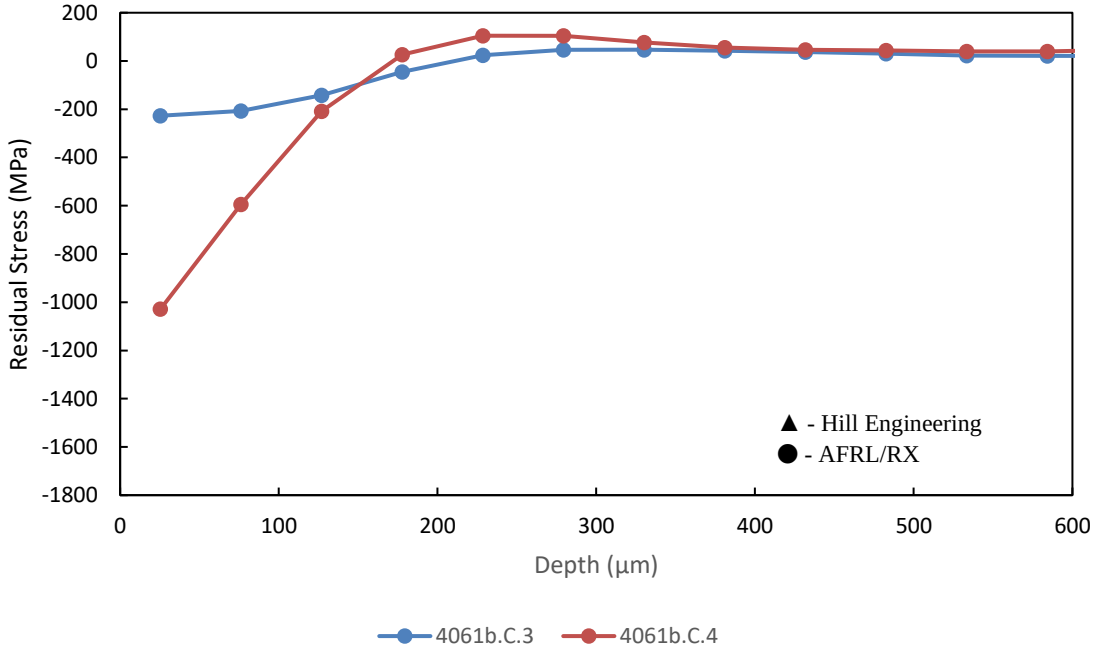

Figure 14 Residual stress profiles after thermal exposure at 538C for 300 hours

There is significant variation between the measurements for the two samples exposed to 538°C for 300 hours seen in Figure 14.The results for 4061b.C.4 are questionable due to a greatly different response than 4061b.C.3. It is believed that this outlier sample may not have been exposed or measured properly, but the data are included for completeness. Due to the questionable nature of these results, it will not be included in further analysis.

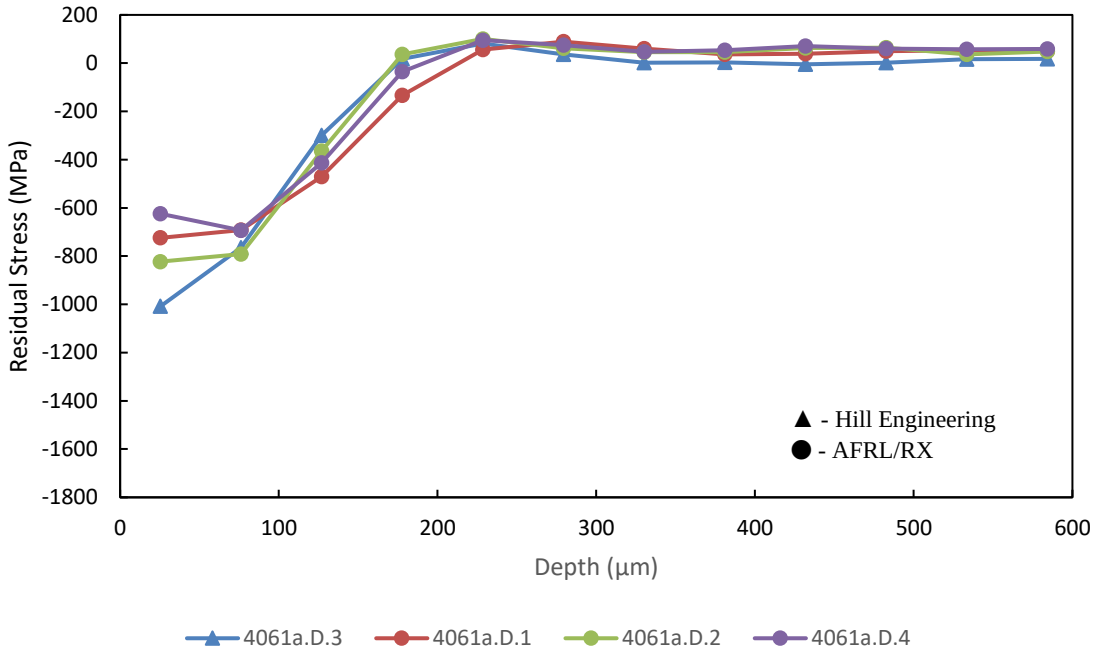

Figure 15 Residual stress profiles after thermal exposure at 650°C for 1 hour

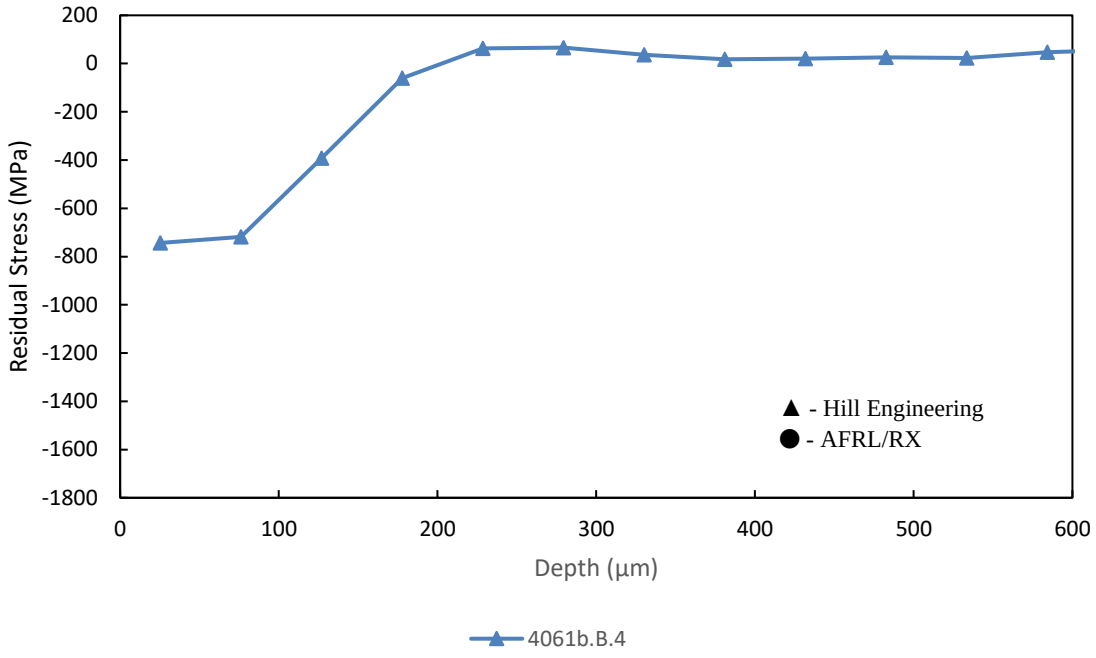

Figure 16 Residual stress profile after thermal exposure at 650°C for 100 hours

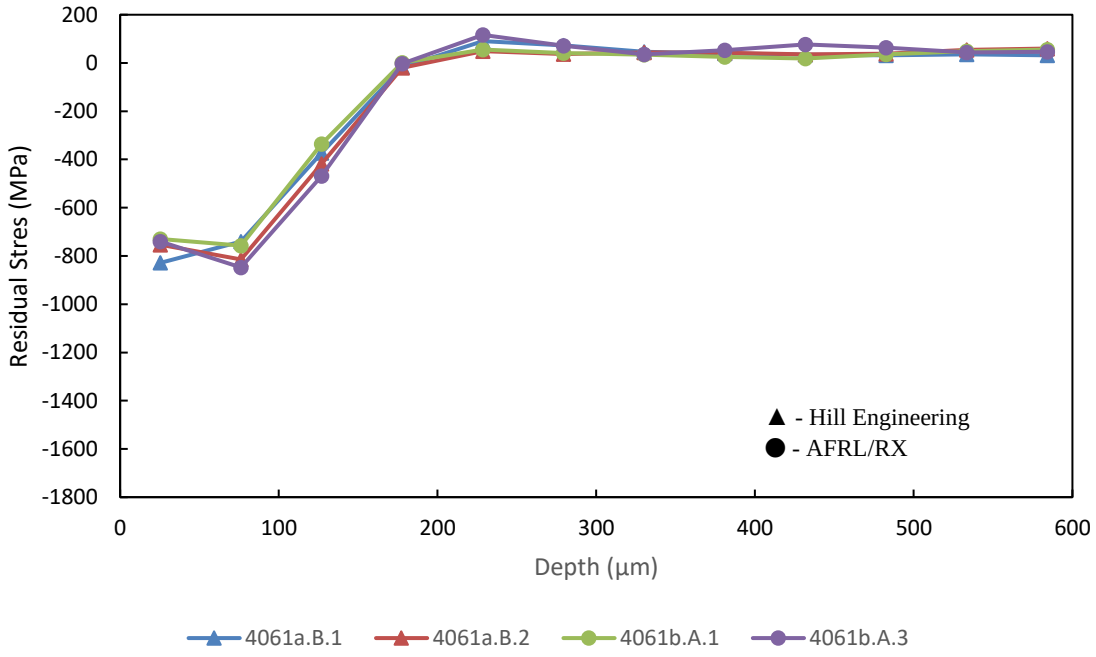

Figure 17 Residual stress profiles after thermal exposure at 704°C for 1 hour

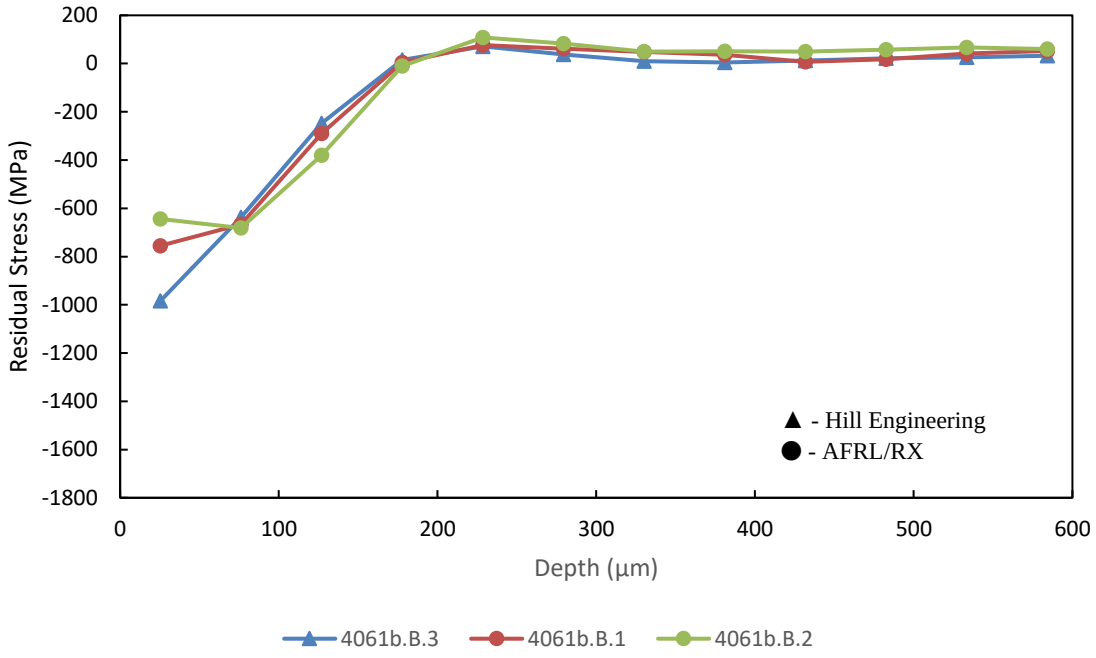

Figure 18 Residual stress profiles after thermal exposure at 704°C for 3 hours

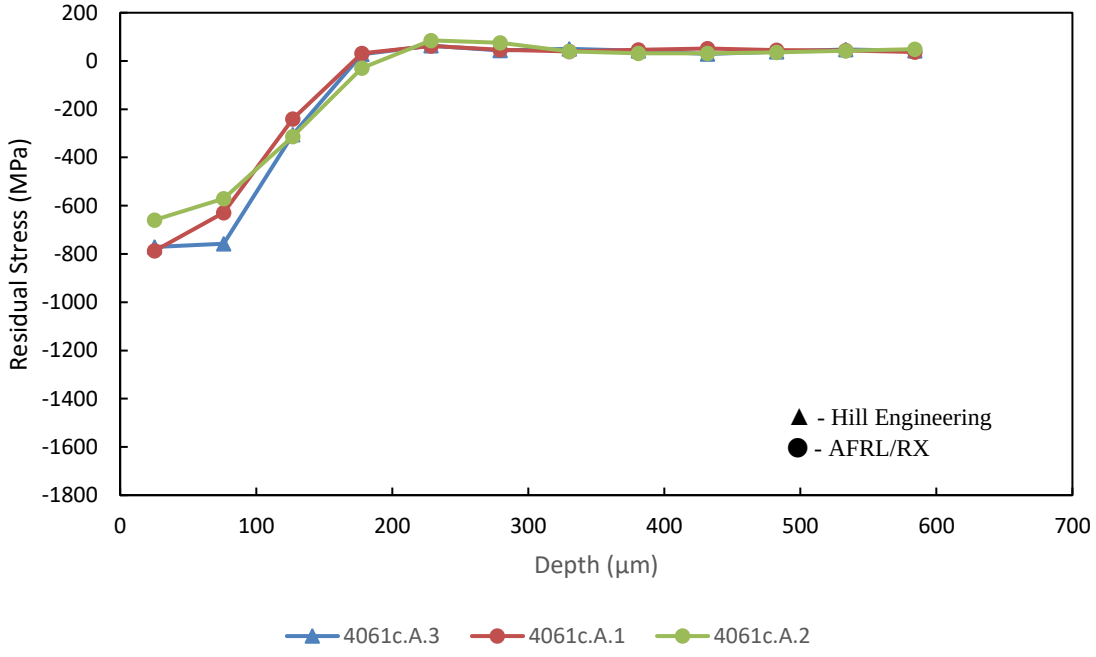

Figure 19 Residual stress profiles after thermal exposure at 704°C for 10 hours

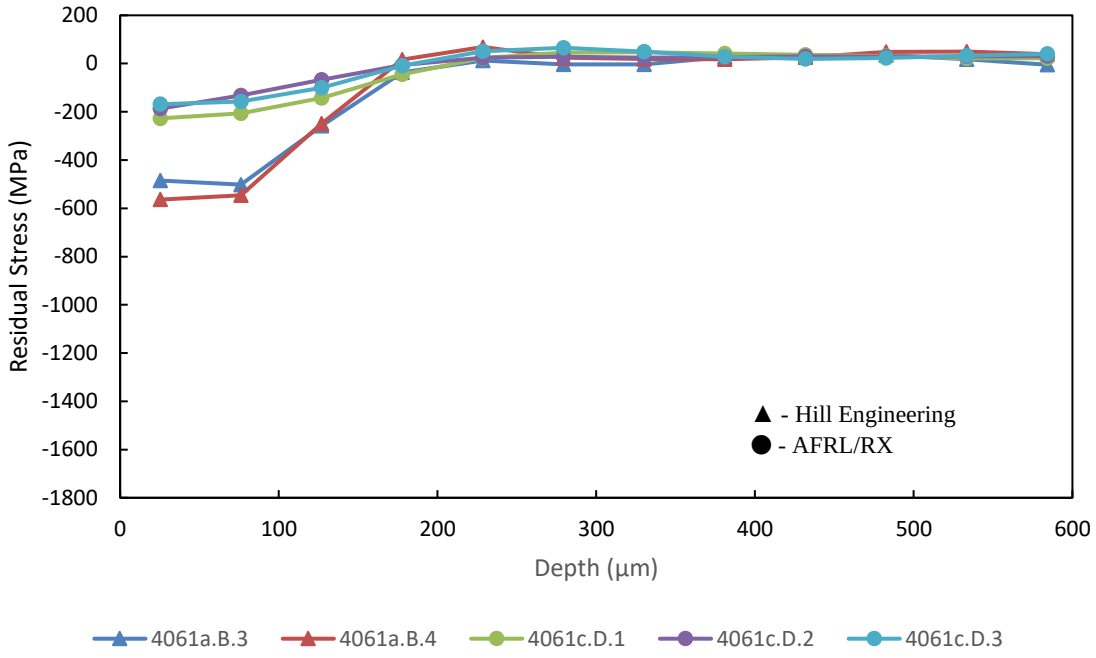

Figure 20 Residual stress profiles after thermal exposure at 704°C for 100 hours

The average residual stress profiles as measured are shown in Figure 21, and the stress profiles after the one hour and 100 hour exposures are shown in Figure 22. The measured residual stress in MPa and the percent relaxation at a depth of 25 µm is shown in Table 4. It is evident that time and temperature are both influential factors on the relaxation of residual stress, as was expected.

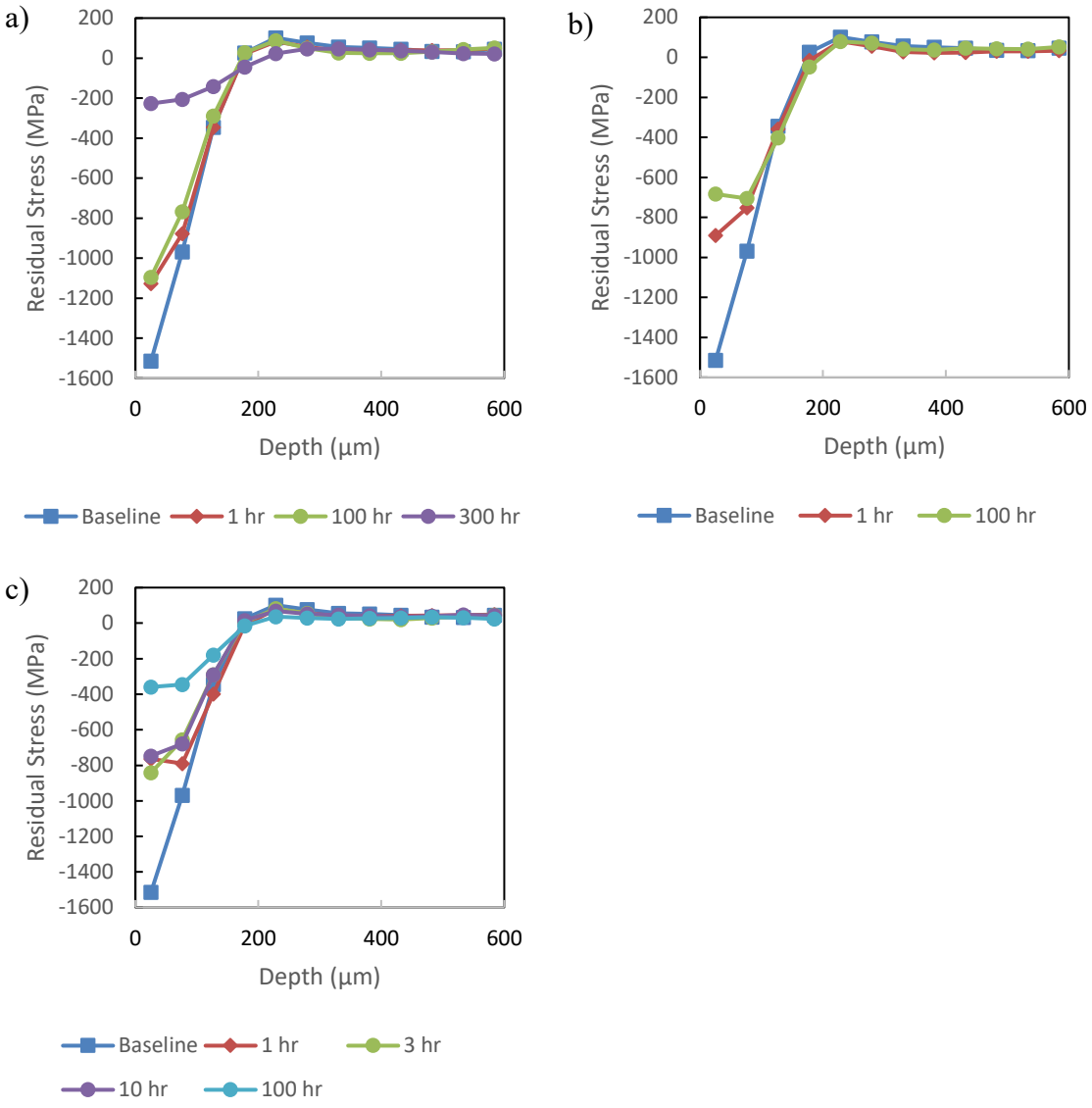

Figure 21 Average residual stress profiles after thermal exposure at a) 538°C, b) 650°C, and c) 704°C

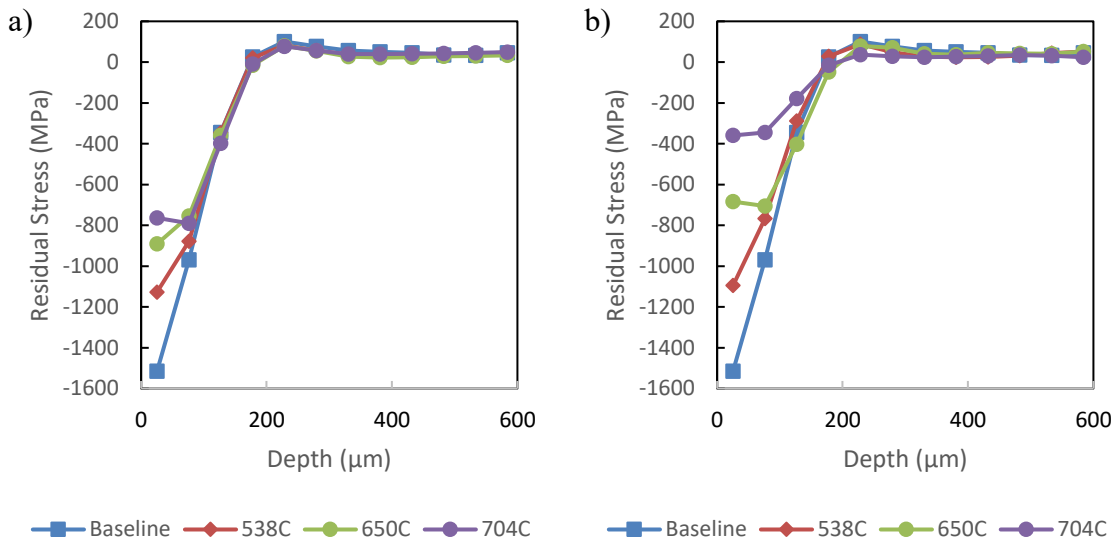

Figure 22 Residual stress profile after a) 1 hour and b) 100 hours

Table 4 Residual stress relaxation after thermal exposure measured with hole drilling method

	1 hr	3 hr	10 hr	100 hr	300 hr
538°C	-1127 (25.6%)			-1095 (27.7%)	
650°C	-891 (41.2%)			-684 (54.8%)	-227 (85%)
704°C	-763 (49.6%)	-842 (44.4%)	-747 (50.7%)	-359 (76.3%)	

However, the thermal relaxation after exposure at 704°C for three hours appears anomalous. The residual stress after that exposure is almost 80 MPa less than after the 1 hour exposure and 95 MPa less than after the 10 hour exposure. It is not likely that both of those results can be true at the same time. The Zener-Wert Avrami function in equations (4) and (5) can provide an analytical tool to help investigate. Equation (4) can be linearized into

$$\log\left(-\ln \sigma_{T,t}^{RS}/\sigma^{RS}\right) = m \log t + m \log A \tag{19}$$

so that $\log\left(-\ln \sigma_{T,t}^{RS}/\sigma^{RS}\right)$ versus $\log t$ can be plotted. This can be seen in Figure 23, along with the best fit lines for 538°C and 704°C exposures already plotted. The regression for 650°C has not yet been conducted because there are only two conditions.

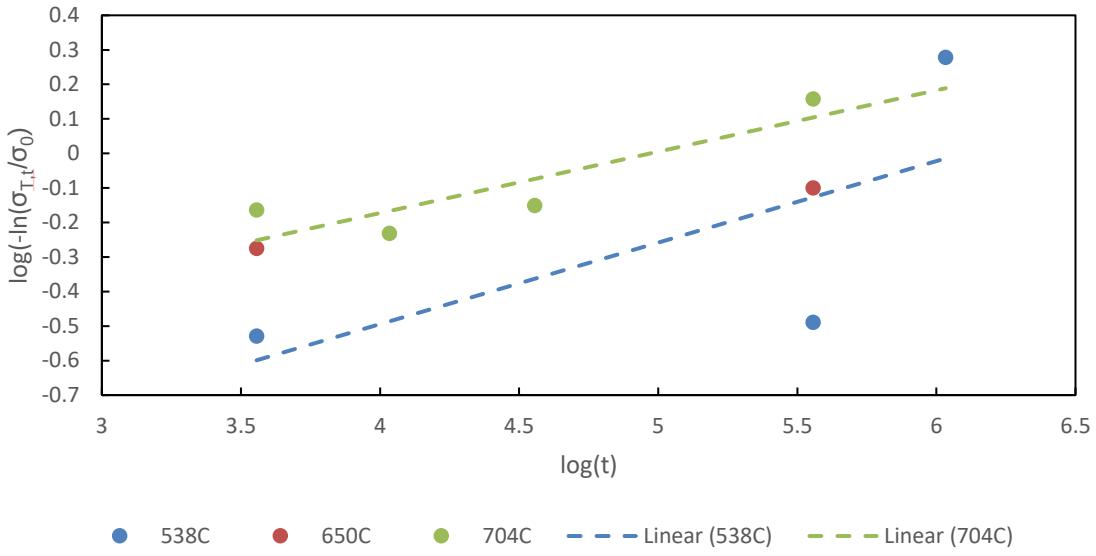

Figure 23 Residual stress ratios plotted against time

These results were calculated from two data sets: one generated by personnel at AFRL/RX and one generated by Hill Engineering. These are plotted separately in Figure 24, along with the regression and the coefficient of determination for exposures at 704°C.

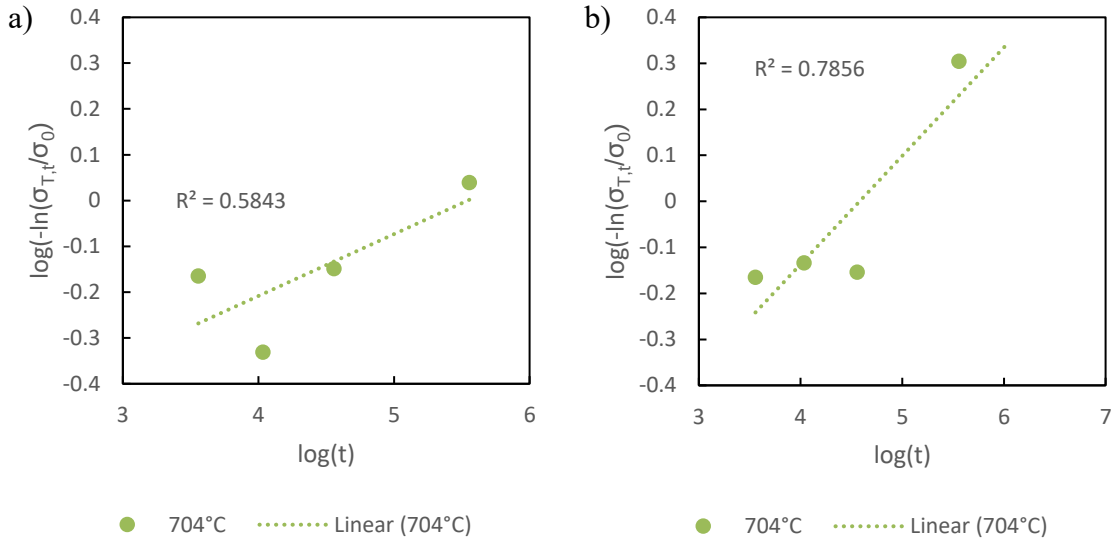

Figure 24 Plots of residual stress ratios vs time for data generated at a) Hill Engineering and b) AFRL/RX

The low value for R^2 for the data from Hill Engineering suggests that the 3 hour exposure may be an outlier. The difference from the 1 hour exposure and the 3 hour exposure is more than three times the reported uncertainty for both measurements. Similarly for the difference between the 3 hour exposure and the 10 hour exposure. See Table 5. The plot of Figure 24a is reproduced in Figure 25, but without the 3 hour exposure from Hill Engineering. The R^2 value increases noticeably. For this reason, this data point is removed from further analysis.

Table 5 Residual stress measurement and calculated uncertainty at a depth of 25 µm

	1 hr	3 hr	10 hr
Measurement (MPa)	-828.5	-983.7	-771.1
Uncertainty (MPa)	50.6	36.5	60.4

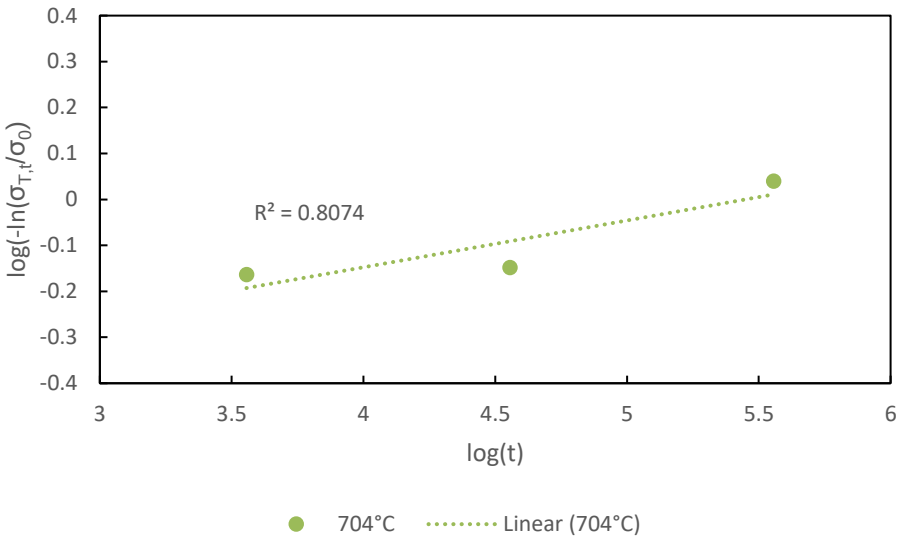

Figure 25 Plot of residual stress ratios vs time for data generated at Hill Engineering without 704°C 3 hour exposure

Figure 23 is reproduced in Figure 26 with three changes: (1) the 704°C 3 hour exposure from Hill Engineering has been removed, (2) the two data sets are plotted

separately, instead of their average, and (3) the regression for the 650°C exposures has been conducted and plotted.

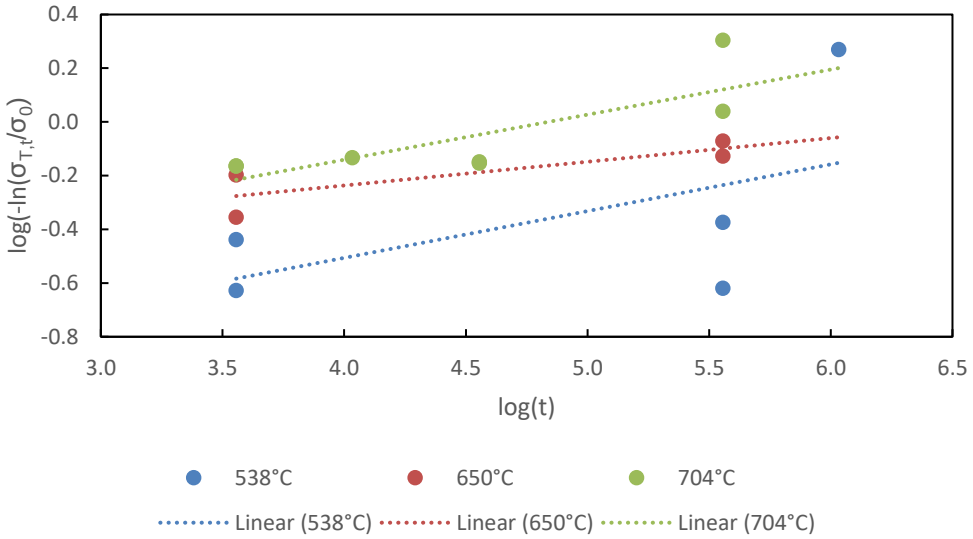

Figure 26 Plot of residual stress ratios plotted against time with data sets separated

Considering again the linearized Zener-Wert-Avrami function, from the plot of $\log(-\ln \sigma_{T,t}^{RS}/\sigma^{RS})$ versus $\log t$, the power m can be found from the slope of the regression lines. They should theoretically be parallel. In Figure 26, regression lines appear parallel for the exposures at 538°C and 704°C, but the line for exposures at 650°C is not parallel. After determining the parameters from the values at 538°C and 704°C, additional exposures can be modeled and checked against the data available. Reproducing equation (19),

$$\log(-\ln \sigma_{T,t}^{RS}/\sigma^{RS}) = m \log t + m \log A \qquad (19)$$

the intercept of the regression line is $m \log A$, and the constant B in equation (5) and the activation enthalpy ΔH can be calculated from this. The slope m and the intercept $m \log A$ for the 538°C and 704°C exposures are shown in Table 6

Table 6 Regression coefficients to determine Zener-Wert-Avrami parameters from hole drilling measurements

	538°C	704°C
m	0.1742	0.1680
$m \log A$	-1.203	-0.8128

To calculate the three unknown Zener-Wert-Avrami parameters, first find the power *m*. This is simply the average of the slopes of the regression lines. Next, the value of A must be determined by dividing $m \log A$ by m and inverting the logarithm. That value is then set equal to equation (5). This is done for both sets of regression coefficients. Then, from equation (5),

$$B = A \exp\left[\frac{\Delta H}{kT}\right] \tag{20}$$

for both sets of regression coefficients. The coefficient B will be same for both sets, so both equations can be set equal, and the activation enthalpy ΔH can be calculated, and the coefficient B solved for. The calculate Zener-Wert-Avrami parameters are tabulated in Table 7, and the full derivation of these parameters shown in **Error! Reference source not found.**. Similarly calculated parameters for Inconel 625 showed an activation enthalpy of 1.59 eV. [28] This indicates that ME3 should have less overall thermal relaxation than Inconel 625, because the energy barrier required for self-diffusion is higher.

Table 7 Zener-Wert-Avrami parameters calculated for hole drilling measurements

B	2457787
ΔH	3.4611×10^{-19} J (2.16 eV)
m	0.1711

Now returning to Figure 26, it possible to check these parameters by modeling a potential exposure condition. Because 650°C is a temperature intermediate to 538°C and 704°C, an

exposure time intermediate to their longest exposures (300 hours and 100 hours, respectively) should yield comparable relaxation. The relaxation predicted for 200 hours at 650°C was added to the data and plotted in Figure 27. The additional point is plotted as a square instead of a circle. Including this point makes the best fit line for 650°C parallel to the best fit lines for the other two temperatures.

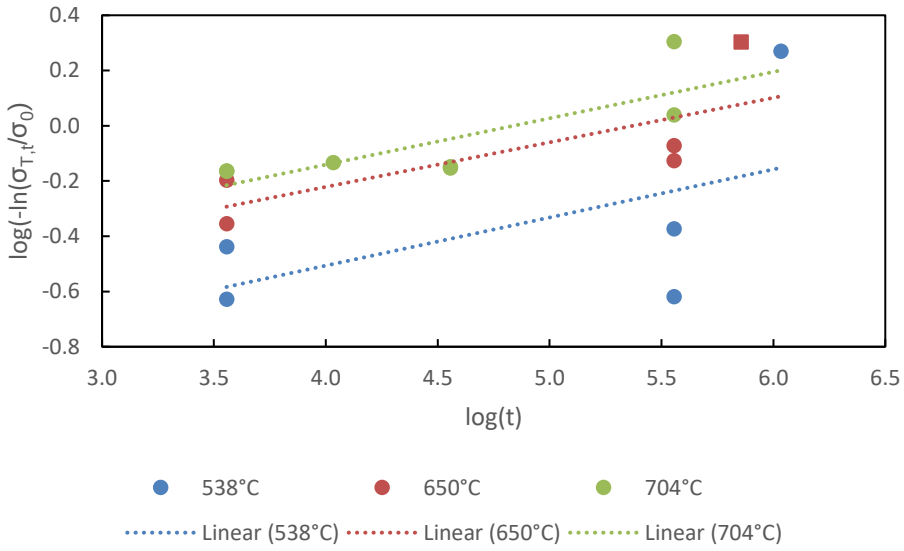

Figure 27 Plot of residual stress ratio against time with additional modeled data for hole drilling measurements

X-Ray Diffraction Results

X-ray diffraction was performed on six samples by Lambda Research, Inc in accordance with SAE HS-784. The residual stress in the 0°, 45°, and 90° directions where determined. [37] The residual stress profiles determined in each direction are shown in Figure 28 through Figure 33. The calculated average profiles are shown in Figure 34.

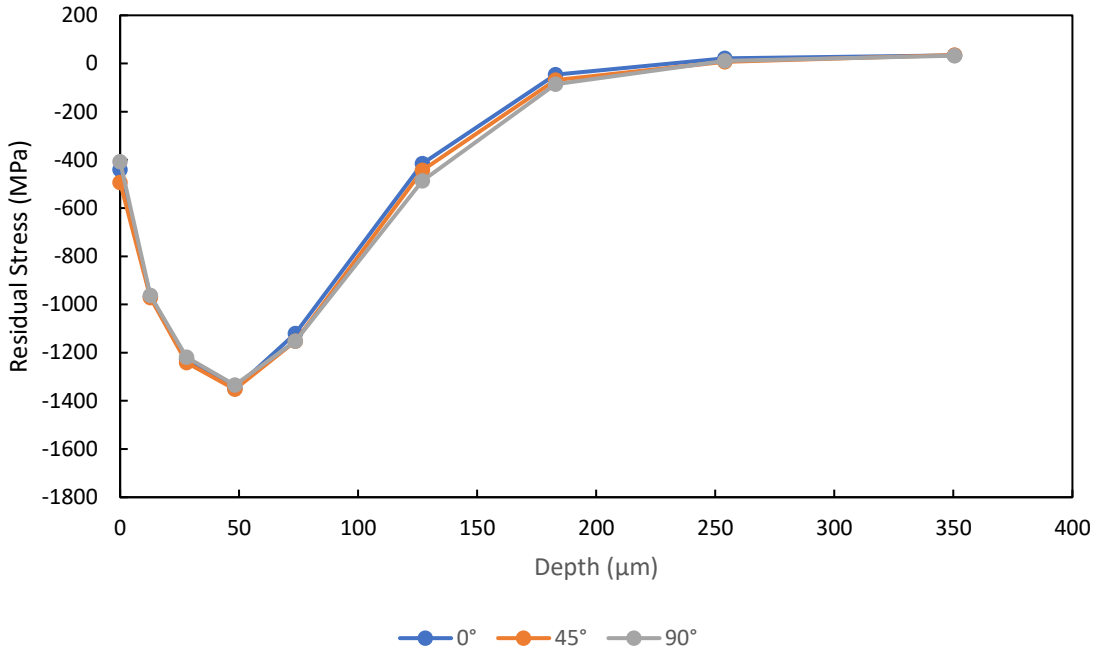

Figure 28 Residual stress profiles for 4061b.D.3 – As Peened

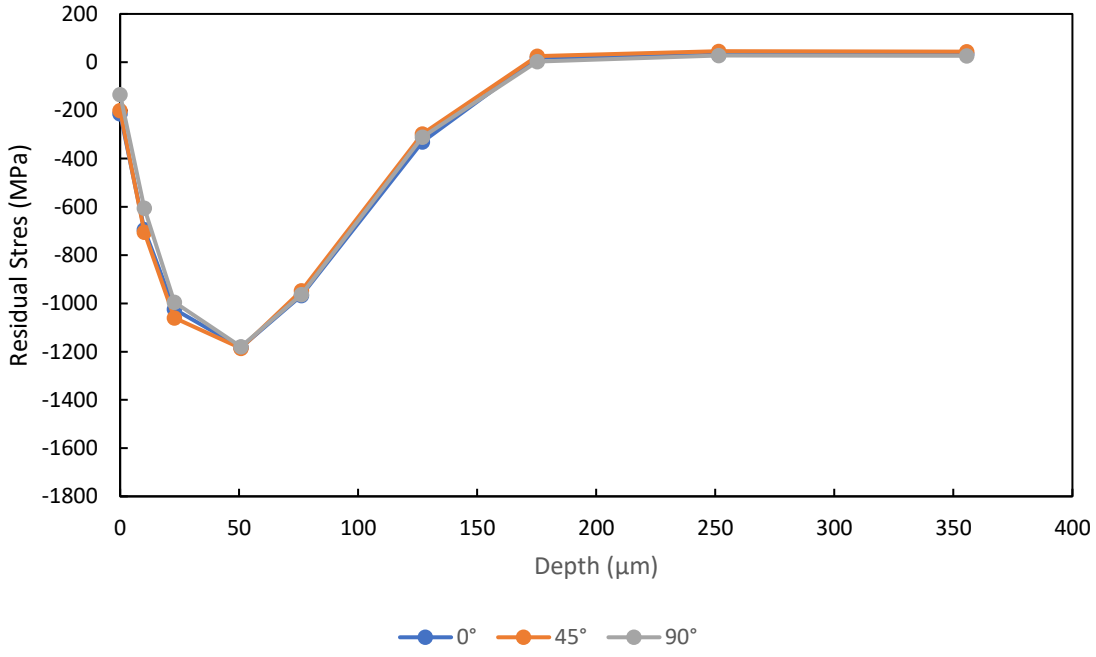

Figure 29 Residual stress profiles for 4061a.C.4 - 538°C 1 hour

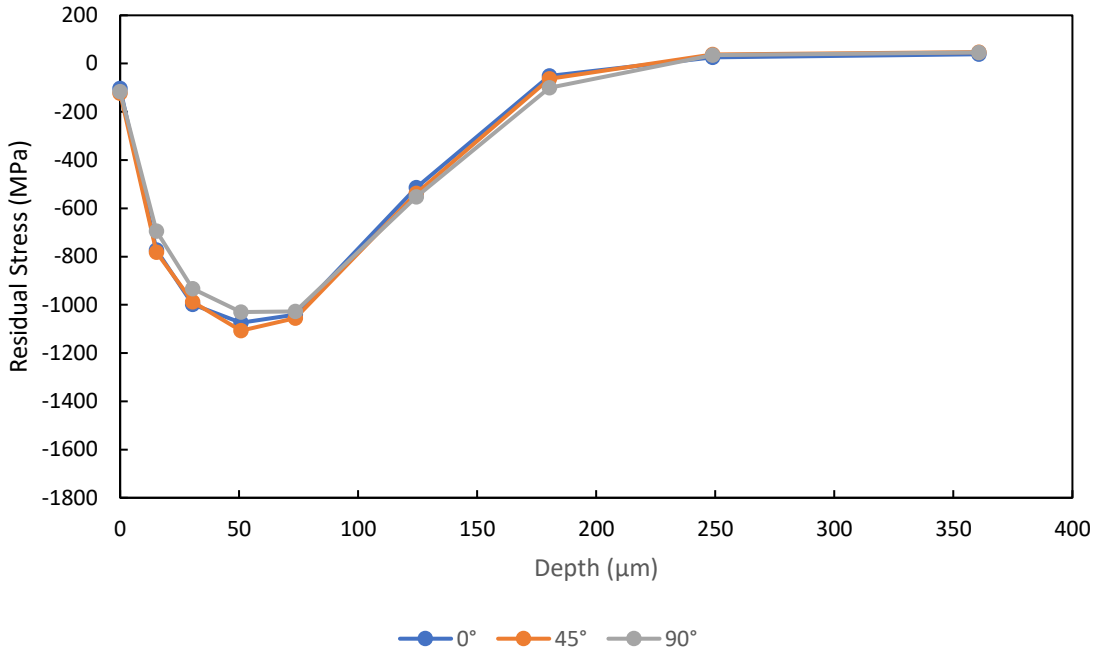

Figure 30 Residual stress profiles for 4061b.C.4 - 538°C 100 hour

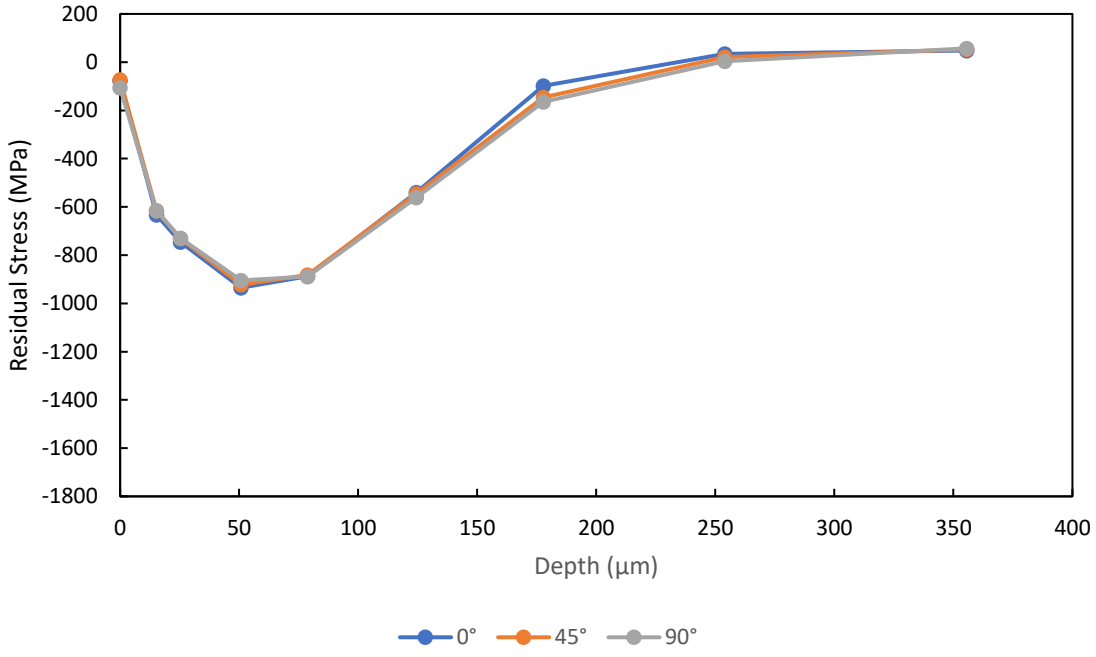

Figure 31 Residual stress profile for 4061c.B.2 - 650°C 100 hour

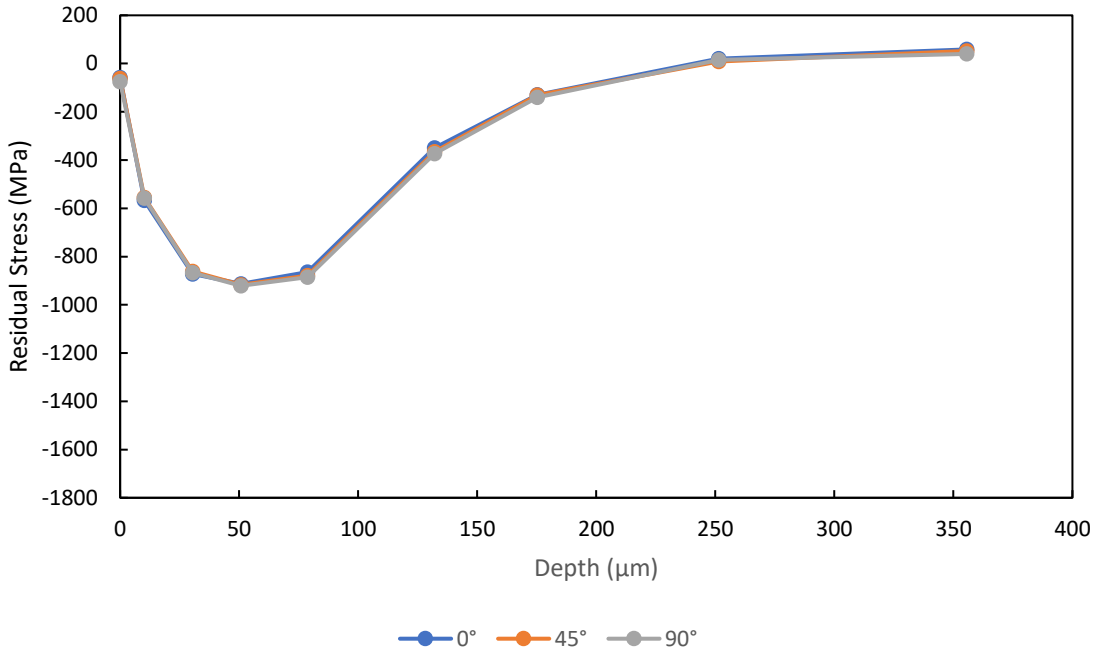

Figure 32 Residual stress profiles for 4061b.A.4 - 704°C 1 hour

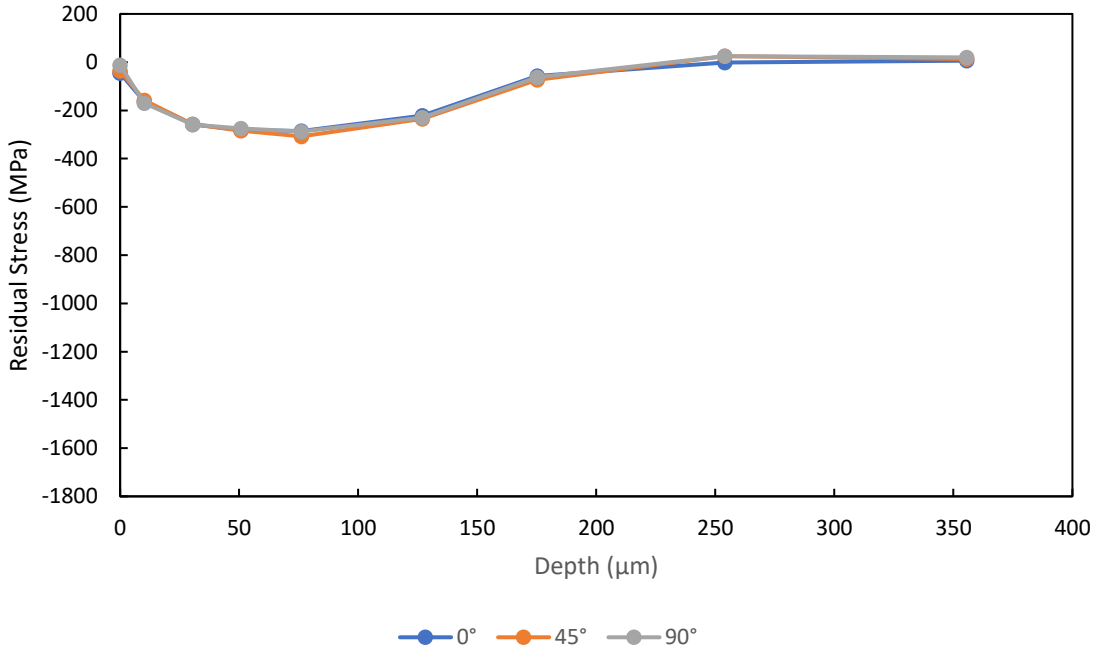

Figure 33 Residual stress profiles for 4061c.D.4 - 704°C 100 hour

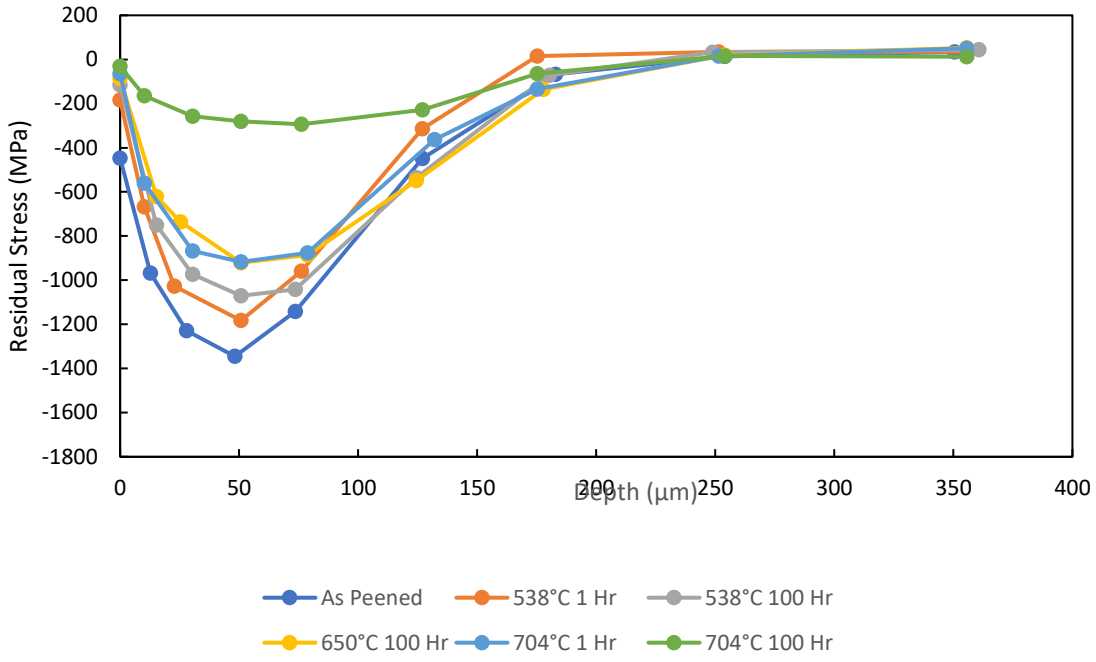

Figure 34 Average residual stress profiles measured by x-ray diffraction

These results are qualitatively typical of residual stress profiles induced by shot peening. The measurements in the different directions are very comparable, as would be expected for shot peened induced residual stresses. The surface magnitude of the surface stresses in MPa and the percent relaxation at the surface are shown in Table 8 and for the maximum residual stress in

Table 9.

Table 8 Surface residual stress relaxation after thermal exposure measured with x-ray diffraction

	1 hr	100 hr
538°C	-182.9 (59.1%)	-114.5 (74.4%)
650°C		-85.5 (80.9%)
704°C	-64.6 (85.6%)	-31.0 (93.1%)

Table 9 Maximum residual stress relaxation after thermal exposure measured with x-ray diffraction

	1 hr	100 hr
538°C	-1182.7 (12.1%)	-1070.5 (20.4%)
650°C		-917.0 (31.8%)
704°C	-917.0 (31.8%)	-293.5 (78.2%))

With these surface measurements, the Zener-Wert-Avrami function can again be used to evaluate the surface relaxation. The plot of $\log\left(-\ln \sigma_{T,t}^{RS}/\sigma^{RS}\right)$ vs log(t) for the x-ray diffraction results is shown in Figure 35. The analysis is the same as previously discussed for the hole-drilling measurements. The regression coefficients used for the analysis are in Table 10, the calculated parameters in Table 11, and the full calculation shown in Appendix B.

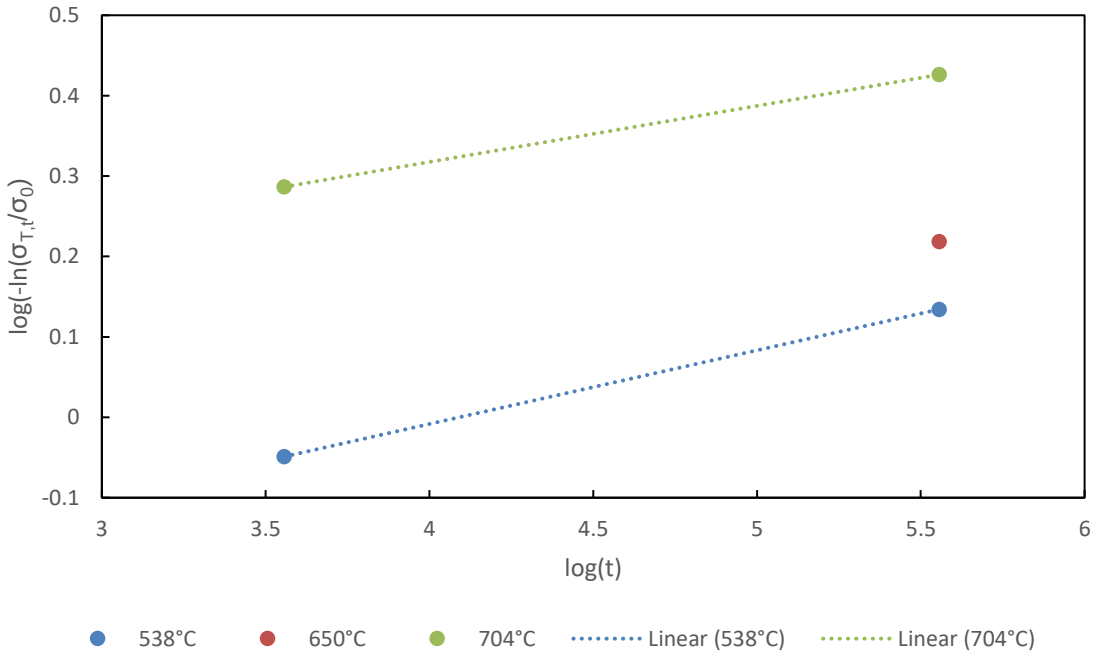

Figure 35 Plot of residual stress ratio against time for x-ray diffraction measurements

Table 10 Regression coefficients to determine Zener-Wert-Avrami parameters from XRD measurements

	538°C	704°C
m	0.0916	0.0698
$m \log A$	-0.3748	0.0385

Table 11 Zener-Wert-Avrami parameters calculated from XRD measurements

B	3.1776×10^{25}
ΔH	7.7739×10^{-19} J (4.85 eV)
m	0.0807

Like with the hole drilling measurements, it is possible to check these parameters with a hypothetical data point. In this case, because the 650°C for 1 hour condition was not measured, that is the condition that will modeled. That data point is calculated and plotted in Figure 36, modeled with a square marker as in Figure 27. The slope of the line joining this modeled data point and the measurement for the 650°C for 100 hours condition is slightly depressed compared to the slope for the lines connecting the two times at the other two temperatures. This could simply just be due to only having two data points to perform the regressions on.

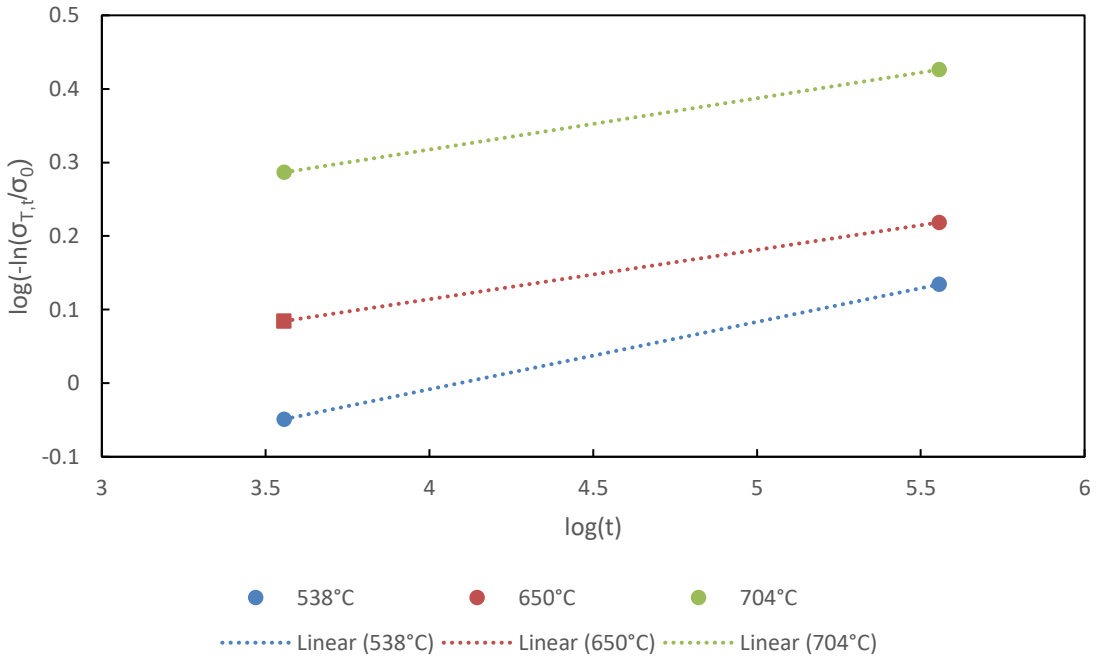

Figure 36 Plot of residual stress ratios against time with additional modeled data for XRD measurements

Because the Zener-Wert-Avrami parameters were calculated from the results of both the hole drilling measurements and the XRD measurements, they can be compared. Table 12 shows these parameters for each measurement method.

Table 12 Comparison of Zener-Wert-Avrami parameters

	Hole Drilling	XRD
B	2457787	3.1776×10^{25}
ΔH	3.4611×10^{-19} J (2.16 eV)	7.7739×10^{-19} J (4.85 eV)
m	0.1711	0.0807

The first thing to notice is how wildly different the coefficient B is. This value is not frequently reported in the literature, so there is no simple way to compare to other nickel base superalloys. The next thing to notice is how the activation enthalpy and the power *m* are inversely related. The activation enthalpy calculated for the XRD measurements is 2.25 times that calculated for the hole drilling measurements. But the power *m* calculated

for the hole drilling measurements is 2.12 times that calculated for the XRD measurements. This is an interesting observation that requires further investigation.

Even though this function does fit the experimental data for both measurement methods well, and can make some predictions, it has its limits. McClung [2] pointed out three principal limitations: (1) it is empirical rather than predictive so that even though it worked in this case, it does not work in every case, (2) the parameter *m* has been observed change with aging temperature, and (3) it has not been extended to thermal relaxation below the surface. This last point is especially important in this case because the first measurement available for the hole drilling method was actually subsurface. Further, as Buchanan [26] pointed out, subsurface behavior cannot be predicted by surface measurements.

With several methods and laboratory facilities used to measure residual stress, it is useful to compare them. The hole drilling results from Hill Engineering and AFRL/RX and the x-ray diffraction results from Lambda are shown in Figure 37 to Figure 42.

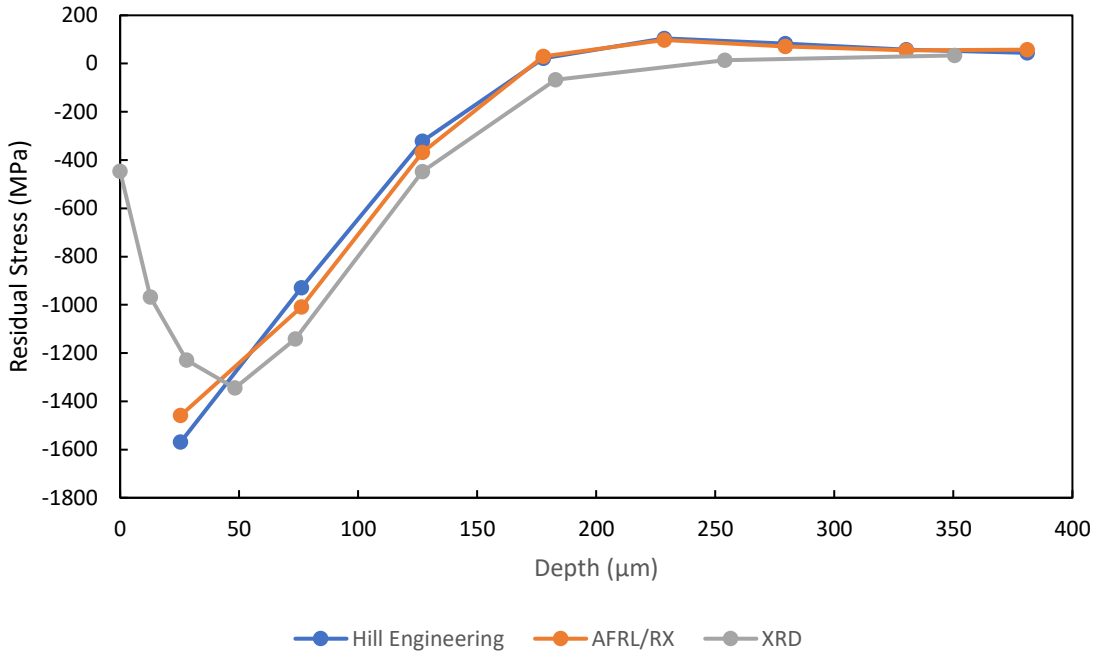

Figure 37 Comparison of hole drilling and XRD results for the as peened condition

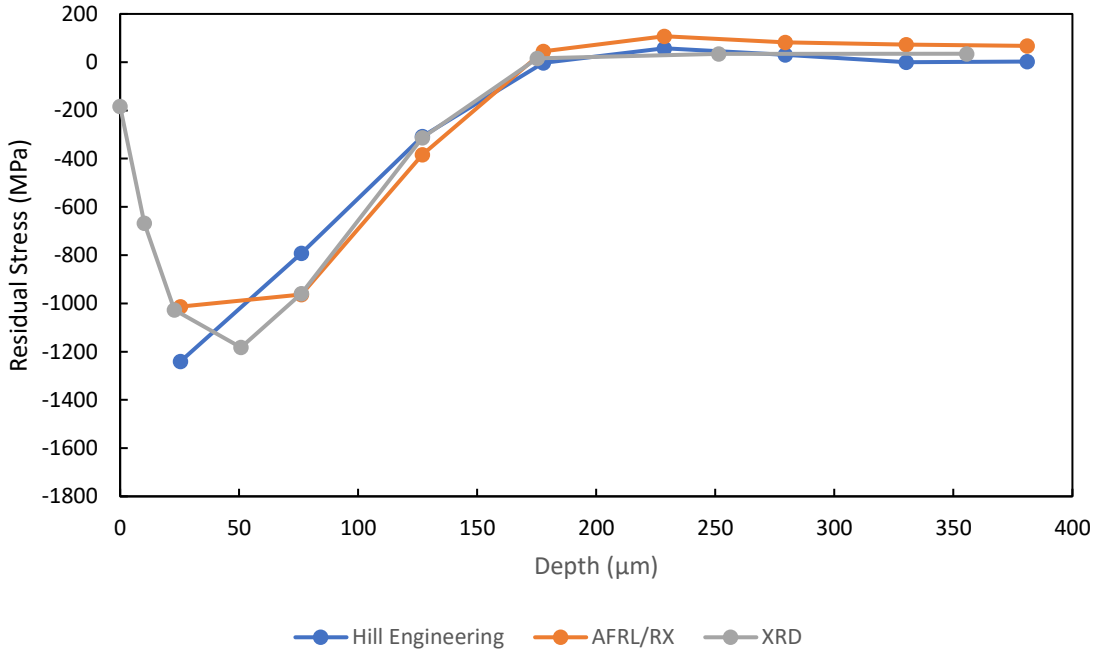

Figure 38 Comparison of hole drilling and XRD results for thermal exposure at 538°C for 1 hour

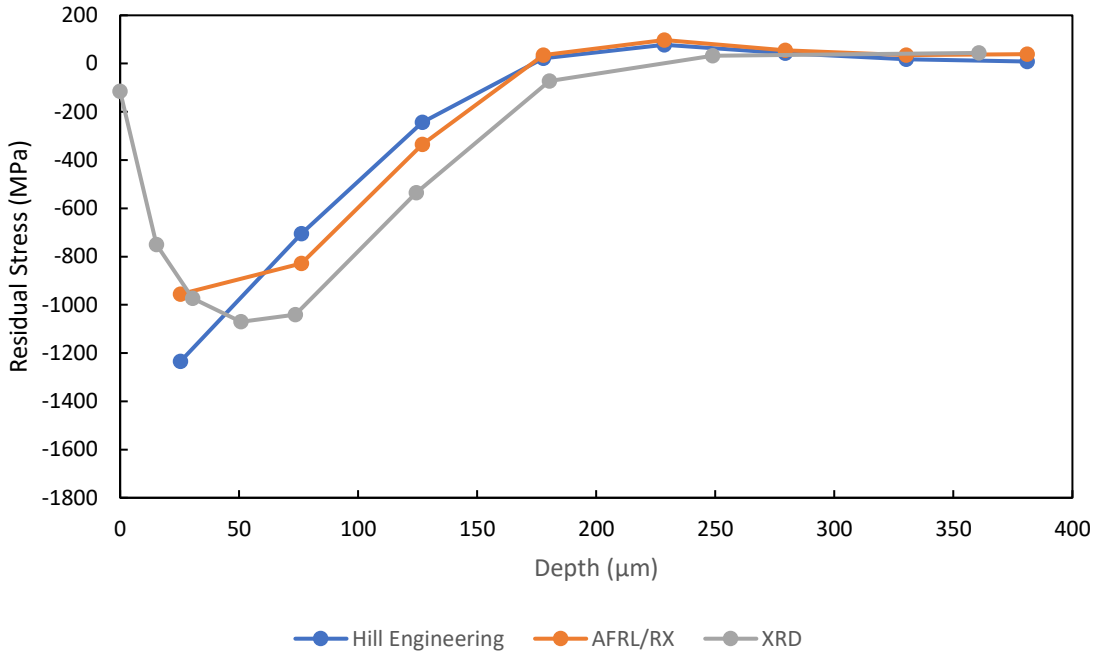

Figure 39 Comparison of hole drilling and XRD results for thermal exposure at 538°C for 100 hour

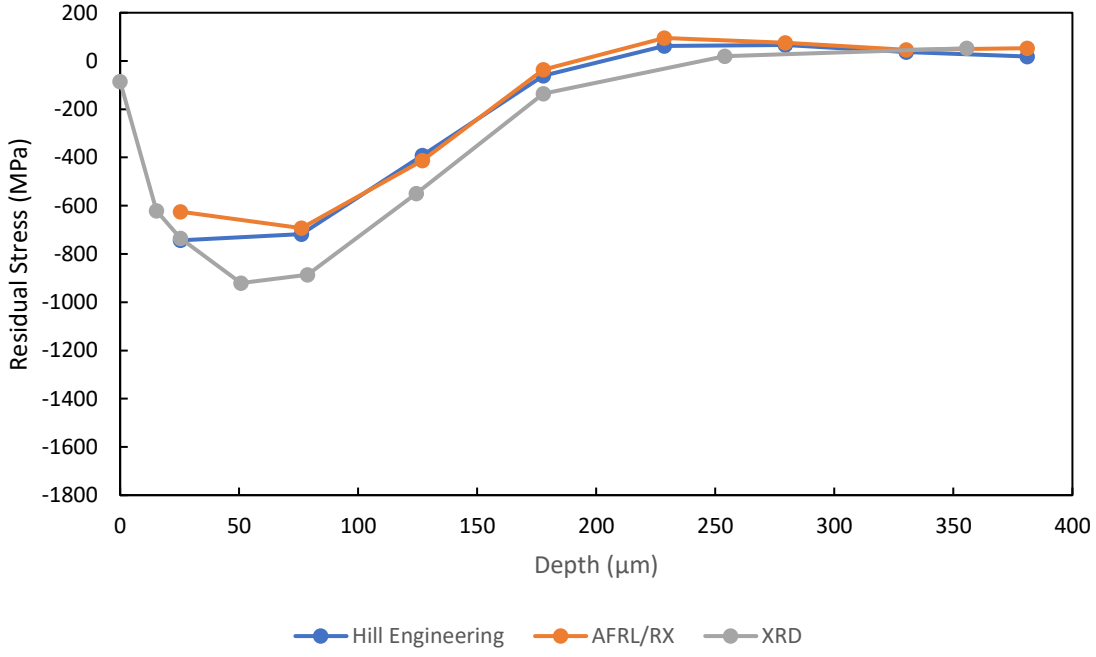

Figure 40 Comparison of hole drilling and XRD results for thermal exposure at 650°C for 100 hours

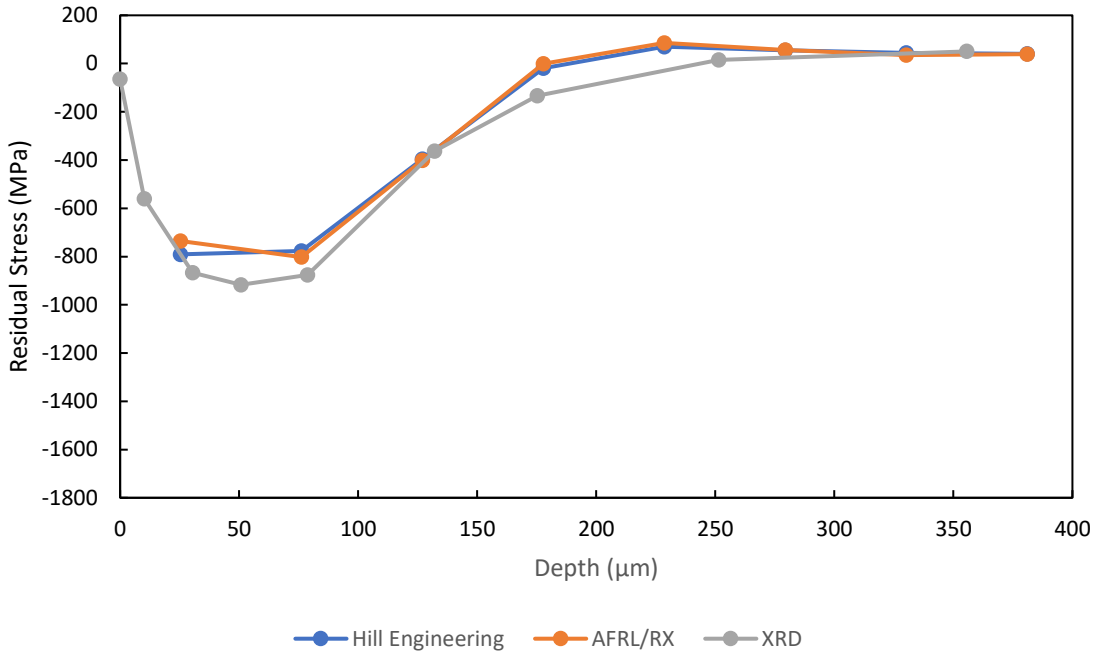

Figure 41 Comparison of hole drilling and XRD results for thermal exposure at 704°C for 1 hour

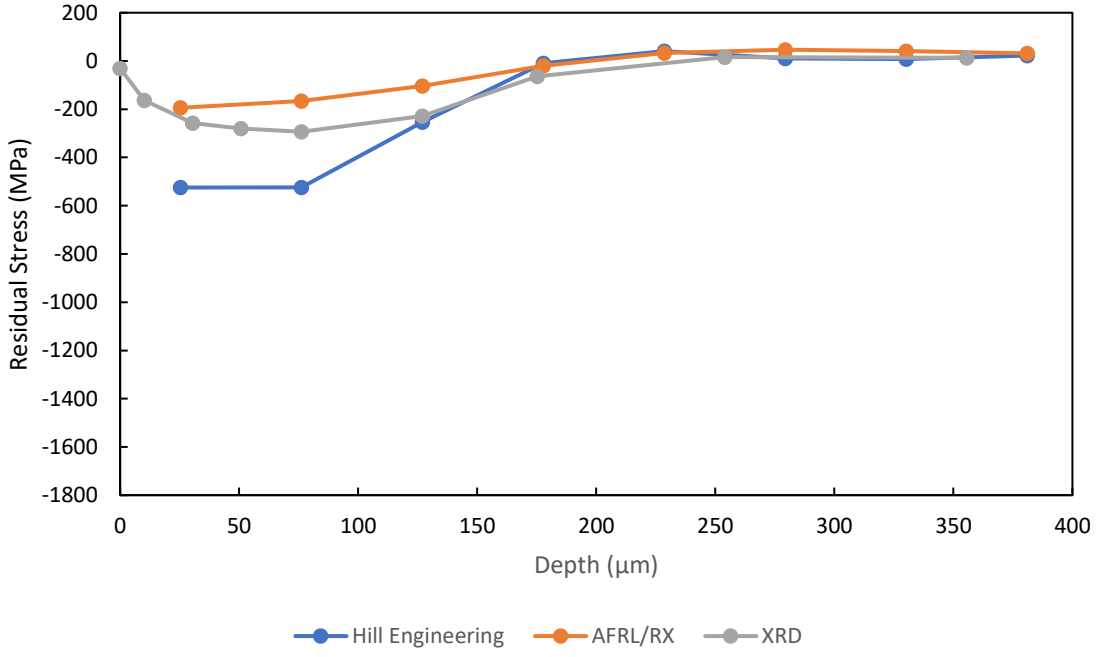

Figure 42 Comparison of hole drilling and XRD results for thermal exposure at 704°C for 100 hours

The error in these measurements is so small compared to the measurements themselves that any error bars would not be visible on the graphs. There is generally good agreement between the x-ray diffraction measurements and the hole drilling measurements. Sometimes the agreement is so good that the data points for the different methods lie on top of each other, such as is the case in Figure 38. The measurements with hole drilling at AFRL/RX and with XRD for that condition are almost the same at depths of about 25 and 75 μm. However, there is an additional XRD measurement at an intermediate depth that is not captured by the hole drilling method. With just the hole drilling method for the size of hole used in this work, that information would be lost. For each hole increment, the reported stress is the average stress through the depth of that increment, rather than the stress measured at the reported depth. That is, at a depth of 25 μm, the reported stress is actually the average stress through a depth of 50 μm. Using a smaller hole would allow measurements to be recorded at smaller intervals, so that this information would be more accurately recorded. Comparatively, X-ray diffraction is able to measure residual stress at particular depths from the surface, including on the surface.

X-ray diffraction is a reliable method of measuring residual stress, which is why it is used so frequently in the literatureHol. But to measure residual stress in parts like the samples used in this work requires specialized lab facilities and specialized training. And to measure a stress profile, the material must be etched away, turning a non-destructive method into a destructive method. The hole drilling method requires some specialized equipment and training, but not quite like what XRD requires. The primary drawback to using the hole drilling method is that it is not possible to get surface measurements. As

the main reason a part would be shot peened is to induce surface residual stresses to prevent crack nucleation, being able to measure on the surface is advantageous.

V. Conclusions and Recommendations

Conclusions

Samples of the nickel-base superalloy ME3 were shot peened to induce compressive residual stress and exposed to a high temperature environment to relax that residual stress. Residual stress was measured using the hole drilling method and with x-ray diffraction. As is typical for this type of work, the residual stress relaxed rapidly early in the exposure periods, and that relaxation slowed down as the exposure went on. The relaxation exhibited dependence on both time and temperature, where comparable results could be achieved by increasing temperature for shorter exposure periods and increasing time for lower exposure time. There is typically good agreement between the hole drilling measurements and the x-ray diffraction measurements, though the hole drilling tended to underestimate residual stress compared to x-ray diffraction, making it a conservative measurement technique. This is beneficial for designers, because if they were to be able to use induced compressive residual stress as a design consideration, it is generally better to be conservative in this way.

The downside to using the hole drilling method is that it is not possible to obtain surface measurements. The maximum residual stress of a shot peened part is typically below the surface, but only at a depth of about 50 μm. Depending on the size of the hole used, that may be the depth of the first hole increment, and the first measurement would be an average of the stress through the depth of that increment. It is not possible to

capture the true residual stress profile with the hole drilling method. This can be mitigated to some degree by using a smaller hole, but the surface residual stresses will never be measured with the hole drilling method.

The Zener-Wert-Avrami function was used to analyze results. The three parameters calculated were very different for each measurement method. This can partially be explained by the fact that the hole drilling results were calculated for residual stresses below the surface, while the Zener-Wert-Avrami function is practically limited to surface measurements. The activation enthalpy for ME3 was calculated to be higher than the activation enthalpy for other nickel base superalloys, which would suggest that it requires more energy input to the system to cause relaxation of residual stress. This would in turn mean that there would be less relaxation of the residual stresses in ME3 than in other nickel base superalloys. However, the amount of data available to calculate the activation enthalpy, along with the other parameters, was barely enough to calculate the regressions (which, for the XRD measurements, was just a line connecting two points).

Understanding the evolution of residual stresses is important for engineers. Compressive residual stresses like those induced through shot peening improve the fatigue life of peened parts. But when those parts are exposed to high temperatures during their service life, such as in a turbine engine where ME3 would expect to be used, the benefits of that residual stress can be lost. The results of this work can be used to further understanding of residual stress relaxation. The measurements taken can be consolidated and used as inputs to more advanced microstructural models to predict the behavior of ME3 in other conditions. It could also be possible to use these results as a baseline for

engineers to estimate residual stresses in shot peened components throughout their lifecycle, so that they could develop more effective inspection intervals. The compressive residual stress would have the result of reducing the maximum stress experienced in a part under cyclic loading, thereby reducing the stress ratio and extending the fatigue life. As the residual stress evolves in a manner like that observed in this work, the fatigue model can be updated.

Recommendations for Future Work

This work was limited in the exposure conditions it was able to investigate and the number of samples it was able to measure. There are many ways that this work could be extended. First would be to continue this work with more exposure conditions. This would allow more accurate calculation of Zener-Wert-Avrami parameters, besides being able to directly track the evolution of residual stress with time and temperature. The same conditions explored in this work should also be investigated with the hole drilling method using a smaller hole. This would result in finer measurement resolution, on the order of 25 μm instead of 50 μm.

Thermal exposure is not the only cause of residual stress relaxation. Mechanical loading will also cause the relaxation of residual stresses. Future work could also include creep and cyclic loading experiments. The effects of thermal and mechanical loading can be measured independently and superimposed. Then, an experiment to measure relaxation under the same thermomechanical loading (i.e., the thermal exposure and mechanical loading at the same time) can be done and compared to the superimposed thermal and mechanical loading results.

Because superalloys such as ME3 are used in applications such as turbine jet engines where the temperature exposure is not constant, an experiment where samples are cycled through temperature changes would be interesting. Such an experiment would place the sample in the furnace at room temperature, ramp up to the operating temperature of a turbine engine, hold steady for a period representing a flight, and then allow the sample to ramp down to room temperature. Because relaxation is proportional to the initial residual stress, it may be possible that, for example, the relaxation experienced after three one hour cycles at temperature may be less than that of one three hour cycle. Or it is possible that, because the total time at elevated temperatures would be longer than the three hour cycle, the three one hour cycles would experience more overall relaxation. This is worth investigating.

Finally, it was observed by the author that equation (5) has a nearly identical form as equation (3). As there was no external loading applied at any point during this work, it is believed that diffusion is the primary cause of thermal relaxation. Thus, it is possible that there is a direct connection between these two equations such that knowing the parameters for one (e.g., the coefficient B and activation enthalpy ΔH in the Zener-Wert-Avrami function) would allow a researcher to easily calculate them for the other (e.g., the diffusion constant D_0 and the activation energy for diffusion ΔQ_d). It may also be the case that there is similar Zener-Wert-Avrami behavior through the depth of the samples, and that the parameters become a function of depth from the surface. Further research into this and other materials could find such relationships.

Appendix A

This section will detail the mathematics required to calculate the Zener-Wert-Avrami parameters shown in Table 7. Equation (19) is reproduced below:

$$\log\left(-\ln \sigma_{T,t}^{RS}/\sigma^{RS}\right) = m\log t + m\log A \tag{19}$$

This equation describes the regression lines shown in Figure 26. The power m is the power is the slope of these lines, which is determined to be 0.1711. The intercept of those lines is the term $m\log A$, and the coefficient B and the activation enthalpy ΔH can be calculated from this. First, the value of A must be determined for each temperature. For 704°C,

$$m\log A_{704°C} = -1.203$$

$$\log A_{704°C} = -7.031$$

$$A_{704°C} = 9.305 \times 10^{-8}$$

And for 538°C,

$$m\log A_{538°C} = -0.813$$

$$\log A_{538°C} = -4.750$$

$$A_{538°C} = 1.774 \times 10^{-5}$$

The term A is given by equation (5), reproduced below, and with the values of A substituted:

$$A = B\exp\left[-\frac{\Delta H}{kT}\right] \tag{5}$$

$$9.305 \times 10^{-8} = B\exp\left[-\frac{\Delta H}{977.15k}\right] \tag{21}$$

$$1.774 \times 10^{-5} = B\exp\left[-\frac{\Delta H}{811.15k}\right] \tag{22}$$

Equations (21) and (22) must be solved simultaneously to calculate the coefficient B and the activation enthalpy ΔH. Therefore, from equation (20), where A has been multiplied by the exponential to solve for B,

$$9.305 \times 10^{-8} \exp\left[\frac{\Delta H}{977.15k}\right] = 1.774 \times 10^{-5} \exp\left[\frac{\Delta H}{811.15k}\right]$$

$$e^{\frac{\Delta H}{977.15k}} e^{-\frac{\Delta H}{811.15k}} = \frac{1.774 \times 10^{-5}}{9.305 \times 10^{-8}}$$

$$e^{200\frac{\Delta H}{k}} = 190.6$$

$$200\frac{\Delta H}{k} = 5.25$$

$$\Delta H = 3.461 \times 10^{-19} \text{ J}$$

This can then be substituted back into equation (20) to calculate B.

Appendix B

This section will detail the mathematics required to calculate the Zener-Wert-Avrami parameters shown in Table 11. The calculations are the same as for those in Appendix A. The slope *m* is 0.0807. Find the value of A for each temperature. For 538°C,

$$m \log A_{538°C} = -0.3748$$

$$\log A_{538°C} = -4.6445$$

$$A_{538°C} = 2.2675 \times 10^{-5}$$

For 704°C,

$$m \log A_{704°C} = 0.0385$$

$$\log A_{704°C} = 0.4769$$

$$A_{704°C} = 2.9984$$

Substituting these values for A into equation (5) and setting them equal:

$$2.2675 \times 10^{-5} = B\exp\left[-\frac{\Delta H}{811.15k}\right]$$

$$2.9984 = B\exp\left[-\frac{\Delta H}{977.15k}\right]$$

$$2.2675 \times 10^{-5} \exp\left[\frac{\Delta H}{811.15k}\right] = 2.9984 \exp\left[\frac{\Delta H}{977.15k}\right]$$

$$e^{\frac{\Delta H}{977.15k}} e^{-\frac{\Delta H}{811.15k}} = \frac{2.2675 \times 10^{-5}}{2.9984}$$

$$e^{200\frac{\Delta H}{k}} = 132236$$

$$\Delta H = 7.7739 \times 10^{-19} \text{ J}$$

Bibliography

[1] Kirk, D. “Shot Peening.” *Aircraft Engineering and Aerospace Technology an International Journal*, Vol. 77, No. 4, 1999, pp. 349–361.

[2] McClung, R. C. “A Literature Survey on the Stability and Significance of Residual Stresses during Fatigue.” *Fatigue and Fracture of Engineering Materials and Structures*, Vol. 30, No. 3, 2007, pp. 173–205. https://doi.org/10.1111/j.1460-2695.2007.01102.x.

[3] Erickson, G. L. Polycrystalline Cast Superalloys. ASM International Metals Handbook: Volume 1, ASM International, pp. 981–994.

[4] Stoloff, N. S. Wrought and P/M Superalloys. Properties and Selection: Irons, Steels, and High-Performance Alloys, ASM International, , 2018, pp. 950–980.

[5] Mankins, W. L., and Lamb, S. Nickel and Nickel Alloys. ASM International Metals Handbook, ASM International, pp. 428–445.

[6] Weber, J. H. Nickel-Based Superalloys: Alloying. Encyclopedia of Materials: Science and Technology, Elsevier, , 2001, pp. 6146–6149.

[7] Weber, J. H. Nickel-Based Superalloys: Alloying Methods and Thermomechancial Processing. Encyclopedia of Materials: Science and Technology, Elsevier, , 2001, pp. 6149–6153.

[8] Noyan, I. C., and Cohen, J. B. The Nature of Residual Stress and Its Measurement. In *Sagamore Army Materials Research Conference Proceedings entitled Residual Stress and Stress Relaxation* (E. Kula and V. Weiss, eds.), 1981, pp. 1–17.

[9] Wohlfahrt, H. Shot Peening and Residual Stress. In *Sagamore Army Materials Research Conference Proceedings entitled Residual Stress and Stress Relaxation* (E. Kula and V. Weiss, eds.), 1981, pp. 71–91.

[10] Callister, W. D., and Rethwisch, D. G. *Materials Science and Engineering: An Introduction*. John Wiley & Sons, Inc., 2010.

[11] Wagner, L. "Mechanical Surface Treatments on Titanium, Aluminum and Magnesium Alloys." *Materials Science and Engineering A*, Vol. 263, No. 2, 1999, pp. 210–216. https://doi.org/10.1016/s0921-5093(98)01168-x.

[12] Champaigne, J. *Shot Peening Overview*. Mishawaka, USA, 2001.

[13] What Is Shot Peening and How Does It Work. https://straaltechniek.net/en/shot-peening-and-blasting-knowledge/shot-peening-knowledge/.

[14] George, T. J., Shen, M. H. H., Scott-Emuakpor, O., Nicholas, T., Cross, C. J., and Calcaterra, J. "Goodman Diagram via Vibration-Based Fatigue Testing." *Journal of Engineering Materials and Technology, Transactions of the ASME*, Vol. 127, No. 1, 2005, pp. 58–64. https://doi.org/10.1115/1.1836791.

[15] Rossini, N. S., Dassisti, M., Benyounis, K. Y., and Olabi, A. G. "Methods of Measuring Residual Stresses in Components." *Materials and Design*, Vol. 35, 2012, pp. 572–588. https://doi.org/10.1016/j.matdes.2011.08.022.

[16] Löhe, D., and Vöhringer, O. Stability of Residual Stresses. In *Handbook of Residual Stress and Deformation of Steel* (G. E. Totten, M. A. H. Howes, and T. Inoue, eds.), ASM International, 2002, pp. 54–69.

[17] Shrestha, D., Azarmi, F., and Tangpong, X. W. “Effect of Heat Treatment on Residual Stress of Cold Sprayed Nickel-Based Superalloys.” *Journal of Thermal Spray Technology*, 2021. https://doi.org/10.1007/s11666-021-01284-x.

[18] Bhowmik, A., Wei-Yee Tan, A., Sun, W., Wei, Z., Marinescu, I., and Liu, E. On the Heat-Treatment Induced Evolution of Residual Stress and Remarkable Enhancement of Adhesion Strength of Cold Sprayed Ti-6Al-4V Coatings. *Results in Materials*. https://reader.elsevier.com/reader/sd/pii/S2590048X20300613?token=881483446C97E3E1798B2888D2B67A1FA69382582DD6E76EF442F39CC9FEFFF54B4AA7913D69B11486D876AC38B3ACD2&originRegion=us-east-1&originCreation=20220111195454. Accessed Jan. 10, 2022.

[19] Cui, X., Zhang, S., Wang, C., Zhang, C. H., Chen, J., and Zhang, J. B. “Effects of Stress-Relief Heat Treatment on the Microstructure and Fatigue Property of a Laser Additive Manufactured 12CrNi2 Low Alloy Steel.” *Materials Science and Engineering: A*, Vol. 791, 2020, p. 139738. https://doi.org/10.1016/J.MSEA.2020.139738.

[20] Chao, Q., Thomas, S., Birbilis, N., Cizek, P., Hodgson, P. D., and Fabijanic, D. “The Effect of Post-Processing Heat Treatment on the Microstructure, Residual Stress and Mechanical Properties of Selective Laser Melted 316L Stainless Steel.” *Materials Science and Engineering: A*, Vol. 821, 2021, p. 141611. https://doi.org/10.1016/J.MSEA.2021.141611.

[21] Ohring, M. Kinetics of Mass Transport and Phase Transformation. In *Engineering Materials Science*, Academic Press, 1995.

[22] Gabb, T. P., Garg, A., Ellis, D. L., and O'Connor, K. M. *Detailed Microstructural Characterization of the Disk Alloy ME3*. 2004.

[23] Gabb, T. P., Telesman, J., Kantzos, P. T., and O'Connor, K. *Characterization of the Temperature Capabilities of Advanced Disk Alloy ME3*. Publication TM-2002-211796. 2002.

[24] Sudbrack, C. K., Evans, L. J., Garg, A., Perea, D. E., and Schreiber, D. K. "Characterization of Grain Boundaries and Associated Minor Phases in Disk Alloy ME3 Exposed at 815 °c." *Proceedings of the 13th International Symposium on Superalloys*, 2016, pp. 927–936. https://doi.org/10.1002/9781119075646.ch99.

[25] Gayda, J., and Kantzos, P. *Burst Testing and Analysis of Superalloy Disks With a Dual Grain Microstructure*. Publication TM-2006-214462. 2006.

[26] Buchanan, D. J., John, R., and Ashbaugh, N. E. "Thermal Residual Stress Relaxation in Powder Metal IN100 Superalloy." *ASTM Special Technical Publication*, Vol. 1497 STP, No. 5, 2008, pp. 47–57. https://doi.org/10.1520/stp45325s.

[27] Foss, B. J., Gray, S., Hardy, M. C., Stekovic, S., McPhail, D. S., and Shollock, B. A. "Analysis of Shot-Peening and Residual Stress Relaxation in the Nickel-Based Superalloy RR1000." *Acta Materialia*, Vol. 61, No. 7, 2013, pp. 2548–2559. https://doi.org/10.1016/j.actamat.2013.01.031.

[28] Wu, L., and Jiang, C. "Effect of Thermal Relaxation on Residual Stress and Microstructure in the Near-Surface Layers of Dual Shot Peened Inconel 625." *Research Article Advances in Mechanical Engineering*, Vol. 10, No. 10, 2018, p. 2018. https://doi.org/10.1177/1687814018800530.

[29] Chin, K. S., Idapalapati, S., and Ardi, D. T. “Thermal Stress Relaxation in Shot Peened and Laser Peened Nickel-Based Superalloy.” *Journal of Materials Science and Technology*, Vol. 59, 2020, pp. 100–106. https://doi.org/10.1016/j.jmst.2020.03.059.

[30] Metal Fatigue Improvement With Stress Waves. https://www.lsptechnologies.com/resources/metal-fatigue-improvement-with-stress-waves/.

[31] METALLIC TEST SPECIMEN PREPARATION, LOW STRESS.

[32] Schajer, G. S., and Whitehead, P. S. *Hole-Drilling Method for Measuring Residual Stresses*. Morgan & Claypool, 2018.

[33] ASTM. E837 Standard Test Method for Determining Residual Stresses by the Hole-Drilling Strain-Gage Method. 1–16.

[34] Micro-Measurements. Instruction Bulletin B-127 Strain Gage Installations with M-Bond 200 Adhesive. http://www.vishaypg.com/docs/11127/11127B127.pdf.

[35] Our Work - DART Automated Residual Stress Measurement. https://hill-engineering.com/case-study/dart-automated-residual-stress-measurement/.

[36] DeWald, A. T., Hill, M. R., Summer, E., Watanabe, B., and Wong, T. Systems and Methods for Analysis of Material Properties of Components and Structures Using Machining Processes to Enable Stress Relief in the Material Under Test, 10,900,768 B2, 2021.

[37] Lachtrupp, T. P., and Kosko, L. *X-Ray Diffraction Determination of the Residual Stress Distribution in Six ME3 Test Blocks*. Publication 25821. Cincinnati, OH, 2022.

Vita

Captain Bryce E. Van Velson graduated from Seward High School in Seward, Nebraska. He entered undergraduate studies at the University of Nebraska – Lincoln where he graduated with a Bachelor of Science in Mechanical Engineering in December 2015. He was commissioned through AFROTC Detachment 465 at the University of Nebraska – Lincoln.

His first assignment was at Tinker AFB as a Developmental Engineer in the 448th Supply Chain Management Wing in January 2016. In February 2018, he was assigned to the B-1 System Program Office, also at Tinker AFB, serving as an aircraft structural engineer. During this time, he also graduated from Oklahoma State University in Stillwater, Oklahoma with a Master of Science in Engineering and Technology Management. In October 2019, he deployed as a Depot Liaison Engineer to the 35th Fighter Wing at Misawa AB. In October 2020, he entered the Graduate School of Engineering and Management, Air Force Institute of Technology. Upon graduation, he will be assigned to the Air Force Research Laboratory Materials and Manufacturing Directorate.

REPORT DOCUMENTATION PAGE

Form Approved
OMB No. 074-0188

1. REPORT DATE *(DD-MM-YYYY)*	**2. REPORT TYPE**	**3. DATES COVERED** *(From – To)*
24-03-2022	Master's Thesis	October 2020-Feb 2022

TITLE AND SUBTITLE

Thermal Relaxation of Shot Peen Induced Residual Stresses in a Nickel Base Superalloy

5a. CONTRACT NUMBER

5b. GRANT NUMBER

5c. PROGRAM ELEMENT NUMBER

6. AUTHOR(S)

Van Velson, Bryce E., Captain, USAF

5d. PROJECT NUMBER

5e. TASK NUMBER

5f. WORK UNIT NUMBER

7. PERFORMING ORGANIZATION NAMES(S) AND ADDRESS(S)
Air Force Institute of Technology
Graduate School of Engineering and Management (AFIT/EN)
2950 Hobson Way, Building 640
WPAFB OH 45433-7765

8. PERFORMING ORGANIZATION REPORT NUMBER

AFIT-ENY-MS-22-M-316

9. SPONSORING/MONITORING AGENCY NAME(S) AND ADDRESS(ES)
Air Force Research Laboratory Materials and Manufacturing Directorate
ADDRESS
PHONE and EMAIL
ATTN: POC

10. SPONSOR/MONITOR'S ACRONYM(S)

AFRL/RXCM

11. SPONSOR/MONITOR'S REPORT NUMBER(S)

12. DISTRIBUTION/AVAILABILITY STATEMENT
DISTRUBTION STATEMENT A. APPROVED FOR PUBLIC RELEASE; DISTRIBUTION UNLIMITED.

13. SUPPLEMENTARY NOTES
This material is declared a work of the U.S. Government and is not subject to copyright protection in the United States.

14. ABSTRACT

Shot peening induces compressive residual stresses in components that positively influence fatigue life. Thermal and mechanical loading causes those residual stresses to relax. The hole drilling method and x-ray diffraction is used to measure the thermal relaxation of residual stresses in the nickel-base superalloy ME3.

15. SUBJECT TERMS
Residual Stress; Thermal Relaxation; Superalloys; Hole Drilling Method;

16. SECURITY CLASSIFICATION OF:			**17. LIMITATION OF ABSTRACT**	**18. NUMBER OF PAGES**	**19a. NAME OF RESPONSIBLE PERSON**
a. REPORT	**b. ABSTRACT**	**c. THIS PAGE**			Anthony N. Palazotto, AFIT/ENY
U	**U**	**U**	**UU**	76	**19b. TELEPHONE NUMBER** *(Include area code)* (937) 255-6565, ext xxxx (NOT DSN) (anthony.palazotto@afit.edu)

Standard Form 298 (Rev. 8-98)
Prescribed by ANSI Std. Z39-18